EXPERIMENTAL VERIFICATION OF A SERVOMECHANISM DESIGN BASIS

Bryan B. Brown, Jr.
and
Carl J. Ostertag, Jr.

8854
on spine:

ERC N

1956

[illegible]
E8098

Letter on front cover:

[illegible]

[illegible]

[illegible]
and
[illegible]

This thesis, written by the authors while affiliated with the Instrumentation Laboratory, M. I. T., has been reproduced by the offset process using printer's ink in accordance with the following basic authorization received by Dr. C. S. Draper, Head of Department of Aeronautical Engineering and Director of the Instrumentation Laboratory.

COPY

Dr. C. S. Draper
Head of the Department of Aeronautical Engineering
and Director of the Instrumentation Laboratory

Dear Dr. Draper:

This is to authorize the deposit in the Library of permanent, offset-printed copies of thesis published by the Instrumentation Laboratory in lieu of the ribbon copies normally required.

Sincerely yours,

(signed) W. N. Locke

COPY

EXPERIMENTAL VERIFICATION OF A SERVOMECHANISM DESIGN BASIS

by

Bryan B. Brown, Jr.
Carl J. Ostertag, Jr.

Submitted to the Department of Aeronautical Engineering on May 21, 1956, in partial fulfillment of the requirements for the degree of Master of Science.

ABSTRACT

In "Design Basis for Multiloop Positional Servomechanisms," Lees develops a design method which coordinates the specifications, dynamic characteristics, interferences, and uncertainties. The method considers the generation of torques by the system, and through the concept of frequency-dependent coefficients in the performance equation, suggests certain modifications to the servomechanism to obtain desired performance.

In order to verify the design basis, a positional servomechanism was constructed including several of the modifications suggested by Lees. These modifications included modified velocity signal damping and a modified displacement signal. This investigation presents the results of testing the modified positional servomechanism and compares these results to those results which were predicted by the design basis. Correlation between results was observed and the design basis is verified for the modified servomechanisms tested.

Thesis Supervisor:	Sidney Lees
Title:	Assistant Professor of Aeronautical Engineering

May 21, 1956

Professor Leicester F. Hamilton
Secretary of the Faculty
Massachusetts Institute of Technology
Cambridge 39, Massachusetts

Dear Professor Hamilton:

In accordance with the regulations of the faculty, we hereby submit a thesis entitled Experimental Verification of a Servomechanism Design Basis in partial fulfillment of the requirements for the degree of Master of Science in Aeronautical Engineering.

ACKNOWLEDGMENT

The authors wish to express their appreciation to the personnel of the Instrumentation Laboratory, Massachusetts Institute of Technology, who assisted in the preparation of this thesis. Particular thanks are due to Professor Sidney Lees who as thesis supervisor inspired and guided the investigation.

The graduate work for which this thesis is a partial requirement was performed while the authors were attached to the U. S. Naval Administrative Unit, Massachusetts Institute of Technology.

TABLE OF CONTENTS

LIST OF ILLUSTRATIONS

LIST OF ILLUSTRATIONS (Cont.)

LIST OF ILLUSTRATIONS (Cont.)

LIST OF TABLES

OBJECT

The object of this investigation is to verify by experimental means a proposed servomechanism design basis.

CHAPTER 1

INTRODUCTION

Many current texts on servomechanism design and analysis deal principally with the dynamic properties, and treat load inertia and damping with interferences as a separate problem. In analysis of the dynamic properties, heavy stress is laid on mathematical and graphical procedures, such as transfer locus, polar diagram, and frequency response. Arbitrary or empirical figures of merit such as gain margin, phase margin, and resonance peak values, are cited which only indirectly relate the response to the actual physical properties of inertia, damping, and elastic effects.

Lees (5)[1] suggests a design basis which is based on an examination of the three physical properties above, and takes into account the specifications, dynamic properties, interferences, and uncertainties simultaneously. He examines a positional servomechanism and six modifications of the servomechanism and presents analogue computer studies of various responses for certain input functions. It is the purpose of this investigation to verify by experimental testing that certain of these predicted responses can be obtained.

[1]Underlined numbers in parenthesis refer to Bibliography.

CHAPTER 2

PRESENTATION OF THEORY

Lees (5) presents a design basis which accounts for uncertainties, interferences, and dynamic factors all at the same time. It is based on a general method discussed in Volume II of (6) and is an extension of Newton's Third Law of Motion. An arbitrary point called the torque summing member (tsm) is chosen in the servomechanism and all torques acting on this point are added and set equal to zero. Under any conditions of operation, the performance of the servomechanism can be completely described by the generation of torques due to inertial reaction, velocity damping, elastic restraint, and interferences. Thus

$$\begin{matrix}\text{Inertial} \\ \text{reaction} \\ \text{torque}\end{matrix} + \begin{matrix}\text{Velocity} \\ \text{damping} \\ \text{torque}\end{matrix} + \begin{matrix}\text{Elastic} \\ \text{restraint} \\ \text{torque}\end{matrix} + \begin{matrix}\text{Interference} \\ \text{torque}\end{matrix} = 0 \qquad (1)$$

In symbols this becomes

$$M_{(ir)} + M_{(d)} + M_{(er)} + M_{(intf)} = 0 \qquad (2)$$

The inertial reaction torque is due to the acceleration of mass. In the positional servomechanism, this would include the effect of accelerating such members as motor armature, elements of the gear train, load (controlled member), and other accelerated components, such as signal generators. Velocity damping torque is proportional to velocities of certain components with respect to others. For this discussion, accelerations, velocities, and displacements are taken as angular accelerations, angular velocities, and angular displacements, and they are referred to the load or controlled member. Mass is taken as angular moment of inertia; damping coefficients are taken as proportional to angular velocity; and elastic restraint coefficients are taken proportional to angular displacement, although the discussion is also valid for linear displacements, etc. Torques due to interferences may include unavoidable losses, such as coulomb friction, wind effects on exposed components, or mechanical reactions on cutting tools. All such effects may be referred to the controlled member. The elastic restraint torque is generated mainly by a motor (torque generator (tg)).

A functional representation of a system for which this discussion will be applied is given below:

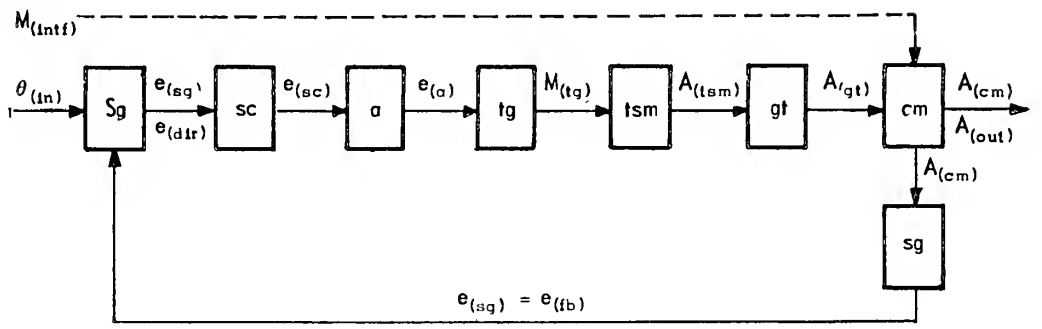

Positional servomechanism functional diagram.

Appendix A contains a derivation of equations for this system and all symbols used are defined therein. The performance equation, Eq. (A-20) in referenced appendix, is based on Eq. (2), and ignoring interference torque is

$$\left[I_{(cm)(eq)}\, p^2 + S_{(ps)[\dot{A};M](res)}\, p + S_{(ps)[A;M]}\right] A_{(cm)} = S_{(ps)[A;M]} A_{(in)} \quad (3)$$

For a sinusoidal input,

$$p = j\,\omega_f \quad (4)$$

Therefore, replacing the operator p by $j\omega_f$, and letting $j = \sqrt{-1}$ and $\omega_f = 2\pi\, n_f = 2\pi/T_f$ = angular forcing frequency, Eq. (4) becomes:

$$\left[-I_{(cm)(eq)}\, \omega_f^2 + S_{(ps)[\dot{A};M](res)}\, j\omega_f + S_{(ps)[A;M]}\right] A_{(cm)} = S_{(ps)[A;M]} A_{(in)} \quad (5)$$

A general consideration of the requirements or specifications for any particular application will govern the choice of torque generator and gear train to be used. Discussions of this selection are available (3) and will not be included here. But in choosing these physical components, certain dynamic properties of the system are thereby established. For if the moment of inertia of the system and load ($I_{(cm)(eq)}$) is considered unchanging and the system elastic coefficient is chosen high enough to overcome interferences and load torque, a reference undamped angular natural frequency $\omega_{(n)(ps)}$ of the system is established. This parameter is defined in Eq. (A-21) of Appendix A, and is the square root of the ratio of elastic coefficient to the moment of inertia. The damping ratio $\zeta_{(ps)(res)}$ is also established (see Eq. (A-24)). $\zeta_{(ps)(res)}$ varies directly with the viscous damping effects of friction in gears and

Again, examining Eq. (5), it is seen that for a ramp input the steady-state response gives

$$p\,A_{(cm)} = p\,A_{(in)} \tag{6}$$

$$p^2\,A_{(cm)} = 0 \tag{7}$$

From Eqs. (5), (6), and (7), it is found that

$$S_{(ps)[\dot{A};M]}\,p\,A_{(in)} + S_{(ps)[A;M]}\,A_{(cm)} = S_{(ps)[A;M]}\,A_{(in)} \tag{8}$$

$$A_{(in)} - A_{(cm)} = -FDE = \frac{S_{(ps)[\dot{A};M]}}{S_{(ps)[A;M]}}\,p\,A_{(in)} \tag{9}$$

where FDE is defined as forced dynamic error. Forced dynamic error may be required to be small for a specified velocity input. On the basis of this requirement and that of restricting velocities in the velocity dominated frequency region described earlier, the velocity damping signal modifier is selected. Many modifiers have been described in the literature. Lees suggests one which is commonly used, and it is shown here in Fig. 5. A performance function and the associated frequency response for this type filter is shown in Fig. 20. This is a nondimensionalized plot in which the velocity signal modifier (vsm) characteristic time is taken as a proportionality constant r_v times the positional servomechanism undamped natural period T.

$$\begin{aligned} \tau_v &= r_v\,T_{(n)(ps)} \quad \text{(dimensional)} \\ \tau_v &= 2\pi\,r_v \quad\quad\quad\;\; \text{(nondimensional)} \end{aligned} \tag{10}$$

By variation of the signal modifier characteristic time-positional servomechanism undamped natural period ratio r_v, more or less velocity damping signal can be passed at a given frequency, while at zero frequency or steady state, no signal will pass, and the FDE

$$FDE = -\frac{\dfrac{\tau_v\,p}{1+\tau_v\,p}\;S_{(ps)[\dot{A};M]} + S_{(ps)[\dot{A};M](res)}}{S_{(ps)[A;M]}}\,p\,A_{(in)} \tag{11}$$

$$\frac{\tau_v\,p}{1+\tau_v\,p} \longrightarrow 0 \quad \text{for} \quad p \longrightarrow 0$$

will be reduced to the minimum possible value. This minimum value would be that of the basic positional servomechanism. Reduction beyond this lower

bearings, air damping, and motor back e.m.f., and inversely with the square root of the product of elastic coefficient and moment of inertia.

Should the transient response of such a system prove too oscillatory, a negative feedback signal proportional to velocity may be added by use of a tachometer. Although this signal has a stabilizing effect and increases the damping ratio, (see Eq. (A-35)), it also has the undesirable effect of causing a greater difference between input angle and output angle during steady-state response to a constant velocity input signal. This is called velocity lag, or forced dynamic error, FDE. At the expense of adding a modifying component the undesired forced dynamic error may be removed.

Before discussing any modification of the system, an examination of Eq. (5) will be made. It is noted that two of the terms in the bracket on the left-hand side are frequency dependent, that is to say, their magnitude varies with the forcing frequency ω_f. For zero frequency, or static conditions, $\omega_f = 0$, and $A_{(cm)}$ is equal to $A_{(in)}$. Since each term in the equation represents a torque, the displacement torque exactly equals the input, and the other torques are zero. This is also approximately true for relatively low frequencies. As ω_f increases, the acceleration torque opposes the displacement torque but is relatively small since it is multiplied by ω_f^2. The velocity dependent torque is 90 degrees out of phase with displacement torque and is also relatively small, since it is multiplied by ω_f. Therefore, for static conditions and the relatively low range of frequencies, it may be said that the system is dominated by elastic effects. As ω_f increases, a point is reached where the acceleration torque is equal to and of opposite sense than the displacement torque. At this frequency the input torque must be balanced by the velocity dependent torque. The velocity torque term is the product of an angular velocity and a coefficient. With a small coefficient, the velocity will be large, and with a large coefficient, the velocity will be small. Therefore, the heretofore unimportant velocity dependent torque has become of prime importance in the velocity dominated frequency region and it appears logical to make the coefficient of this term frequency dependent. A sensible choice would be to make it zero at relatively low frequencies and a maximum in the region where the inertia and elastic reaction torques cancel each other. This is the basis for the modification included in the Modified Velocity Signal Damping Positional Servomechanism (ps)(mvsd) model shown in Fig. 12.

As ω_f increases still more, ω_f^2 becomes much larger, and the acceleration torque term overpowers both the velocity dependent torque and the displacement torque. In this frequency region the system becomes useless for control purposes.

limit is impossible with the components selected, because this minimum FDE is due to bearing friction, air damping, and motor back e.m.f.

Lees presents a series of analogue computer studies of the response of this modified system for displacement step function inputs using various values of damping ratio $\zeta_{(ps)}$ and r_v. These responses taken from (5) are shown in Fig. 22.

Another modification suggested in the design basis is one which reduces FDE and also within the operating limits of the components of the system reduces the static response to interferences to zero. The positional servomechanism incorporating this modification is designated the Modified Displacement Signal, Velocity Signal Damping Positional Servomechanism (ps)(vsd)(mds). It is shown in Fig. 13. Equation (A-26) of Appendix A shows that the response of the basic positional servomechanism (ps)(b) to an interference (here any interference torque is assumed operating on the controlled member) depends on the compliance, which is the reciprocal of the stiffness coefficient. See Eq. (A-25). Thus a reduction in compliance (or an increase in stiffness) will reduce the response to $M_{(intf)}$. An infinite stiffness would reduce the response to zero. Equation (9) shows that infinite stiffness will reduce the FDE to zero. Hence, the basis for this modification is shown. Such a modification is shown on Fig. 24 with its associated frequency response and performance function. The displacement signal modifier (dsm) incorporates a feedforward of the integral of the angular displacement error signal in parallel with the error signal. Such a modifier integrates any error signal, however small, to a large signal after sufficient time. The integrated error causes the motor to generate enough torque through the gear train to drive the angular displacement error to zero. Figure 24 shows the frequency response of the (dsm) to approach infinity at low frequencies, and decrease to its minimum value at $p \to \infty$ since

$$|PF|_{(dsm)} = \frac{1 + \tau_d p}{\tau_d p} \tag{12}$$

$$|PF|_{(dsm)} \to \infty \qquad \text{as } p \to 0$$

$$|PF|_{(dsm)} \to 1 \qquad \text{as } p \to \infty$$

Equation (A-47) of Appendix A and Eq. (9) can be used to show that

$$FDE = - \frac{S_{(ps)[\dot{A};M]} \; p \, A_{(in)}}{S_{(ps)[A;M]} \; \dfrac{1 + \tau_d p}{\tau_d p}} \tag{13}$$

Then by Eq. (12), it can be seen that FDE may be made equal to zero. With this and the fact that the (ps)(vsd)(mds) has zero static response to $M_{(intf)}$, justification for the (dsm) modifier is established. Lees thus makes the stiffness coefficient frequency dependent, and obtains a variation in dynamic characteristics by variation of the (dsm) time constant τ_d. He sets τ_d equal to a proportionality constant r_d times $T_{(n)(ps)}$, relating (dsm) performance to the servomechanism performance.

$$\tau_d = r_d T_{(n)(ps)} \tag{14}$$

Analogue computer studies of the response of the (ps)(vsd)(mds) to position step function inputs and interference torque inputs for various values of damping ratio $\zeta_{(ps)}$ and r_d are presented by Lees. These are taken from (5) and are shown in Fig. 26.

Two other modifications are suggested and studied by Lees but these are not discussed here. The theory as presented has demonstrated that by coordinating the specifications, interferences, and dynamic characteristics, and through the summation of torques generated, frequency dependent coefficients may be selected for appropriate modifiers. With these the system response can be established as desired within the operating limits of the components. Further refinement of the response can be made by any of the current techniques, and stability of the system also may be investigated by other means. But the design basis presents a readily available starting point in design and gives an indication of the variation permissible in changing the system parameters.

This investigation was done in order to verify experimentally that the various responses can in fact be obtained as predicted by the design basis. For this purpose, a positional servomechanism was built incorporating these modifications, and the response of the servomechanism is to be compared with the response predicted by the theory.

CHAPTER 3

DESCRIPTION OF THE EQUIPMENT

In order to verify experimentally the design basis suggested by Lees (5), it was necessary to build the servomechanism and incorporate the required modification. It was assembled from such components as were available at the time at the Instrumentation Laboratory, Massachusetts Institute of Technology, where the investigation was to be conducted. Due to time limitations, only the basic positional servomechanism (ps)(b), the velocity signal damping positional servomechanism (ps)(vsd), the modified velocity signal damping positional servomechanism (ps)(mvsd), and the modified displacement signal, velocity signal damping positional servomechanism (ps)(vsd)(mds) were tested. The first two models are common and their characteristics are well known. Their responses were obtained to indicate that the experimental servomechanism as assembled and operating was in fact the system desired and that their behavior was predictable. With predictable behavior for the (ps)(b) and (ps)(vsd), confidence can be attached to the behavior of the (ps)(mvsd) and (ps)(vsd)(mds) models.

In general, the details of the servo were governed by the components available. These were a two phase alternating current motor, an a-c amplifier, a d-c amplifier, a d-c tachometer, assorted spare gears and shafts, and the potentiometers. Each of these had been removed at some earlier date from computers. The a-c amplifier had been designed to excite the motor. The necessary modifications required by the theory can best be done by operating on a d-c signal. The potentiometers were, therefore, excited with d-c voltage, which was modulated and fed to the a-c amplifier. For the same reason, the d-c tachometer signal was not modulated until after it had been modified where necessary.

Figure 1 shows a pictorial diagram of the servomechanism as finally assembled, including the necessary testing instruments. Figure 2 contains a functional diagram of the servo, and Figs. 3, 4, 5, 6, and 7 illustrate the various components. The Reeves computing amplifier, MK 77, Mod O, was used in the Displacement Signal Modifier, and the Reeves a-c amplifier was

used as the power amplifier to drive the motor, for reasons described above. Descriptions of various components or items follows.

Potentiometers. These were high quality instrument-type potentiometers previously used in an older model Reeves Instrument Company analogue computer. Both potentiometers were identical ten-turn units with a resistance of 20 K ohms each. Prior to installation, each was spot checked for voltage linearity, and with the voltmeter used, no nonlinearity could be detected. Beyond this, no testing was done, because it was assumed that whatever small nonlinearity might exist would be very small compared to nonlinearities of the motor, amplifier, and other items.[2]

The potentiometers were excited by two 45 volt batteries in series.[3] This excitation allowed an error signal level far enough above noise level and yet did not exceed the power dissipation rating of the potentiometers. After assembly of the complete servo, no detectable drop in battery excitation voltage was noted for any trial positions of the individual potentiometer rotors.

Adder and Chopper circuit. This circuit consisted of a resistive adder network feeding a chopper unit, the output of which passed through a transformer. Three functions were performed. The displacement error signal, tachometer feedback signal, and a Servoscope test signal (square wave or sine wave) were added, the sum of the signals became a modulation on the 60 cycle carrier frequency and was passed on as a 100 percent modulated carrier to the a-c amplifier. The third function was that of phase shifter for the 115 volt 60 cycle supply.

The resistor values used caused the displacement error signal and tachometer signal to be added in equal proportions, but the Servoscope signal in a much smaller proportion. The 6 megohm value was selected high to isolate the other two signals from the Servoscope unit.

Figure 8(b) shows how the output voltage (RMS volts) varied with input d-c voltage. The straight line portion gives a slope of 0.1 volt per volt, and it appears that saturation starts at an input of 0.4 volt input.

A-C amplifier. A Reeves Instrument Company A-C amplifier designed for use with the motor was used. Figure 7 shows the wiring diagram. It is a feedback amplifier, three stage, with final stage push-pull. Gain of about 3300 to 33000 was available, but distortion was bad in higher gains. Figure 8(a) shows

[2]Potentiometers of this type can be expected to have a linearity of 99%. See Ahrendt, (4) page 20.

[3]Measured battery voltage was 78 volts.

how gain and phase angle deviated with frequency changes above and below carrier frequency. For the gain used during system testing, (3000 – 4000 gain), not over two or three percent deviation in gain and 5 degrees in phase angle was noted. Tests showed the amplifier to saturate at about 120 volts, and for zero input, the output voltage was 0.8 volt.

Torque generator. A Diehl 7 watt, 2 phase, type SS FPE 25-11 a-c motor was used. Performance characteristics are plotted in Fig. 9. This is test data done by Mr. D. P. Mason of the Instrumentation Laboratory on this particular motor. It has the nonlinear characteristics described for this general type of motor in (3), (4), and (7). Rated voltage for the control field is 75 volts, but no excessive heating was observed as high as 125 volts. Figure 9 indicates no great nonlinearity involved in using a voltage of this magnitude. With

$$S_{(tg)[e;M]} = \left[\frac{\partial M}{\partial e}\right]_{\text{speed constant}} \quad \text{(See Appendix B)} \tag{15}$$

$$S_{(tg)[\dot{A};M]} = \left[\frac{\partial M}{\partial \dot{A}}\right]_{\text{voltage constant}} \tag{16}$$

it can be seen that the two sensitivities vary by factors of 40 percent and 70 percent if voltage is allowed to vary from zero to 115 volts and speed from zero to about 800 RPM as was expected during normal testing described later. Ninety degrees phase separation between control field and reference field voltages was accomplished through the phase shifting of the 60 cycle carrier in the adder-chopper.

Gear train. The gear train was assembled from such used gears as were available. These were 32 teeth per inch pitch aluminum gears except for motor pinion, which was steel. A limit-stop rider was installed on one shaft to protect potentiometers, even though its addition probably increased sticktion and level of friction, and the uncertainty in determining either. No attempt was made to match load inertia to motor inertia by a specific gear train ratio. The ratio resulting was a compromise between space limitations, a desire to use a minimum of meshes and a desire to use small diameter gears so that moments of inertia would not be large. The gear train ratio motor to controlled member was 17.35 and motor to tachometer was 12.82. Backlash between motor and controlled member was measured to be no more than ±1/2 milliradian.

Controlled member. A pulley wheel with cross arm fixed to it and a mirror were the controlled member which constituted the load. A weighted pan was attached to the pulley wheel by a string for torque application. Two springs

were attached between the cross arm and the base for use in determination of the moment of inertia and residual viscous effects. This test is described in Chapter 4. The mirror reflected a light beam from a source (source had built-in cross hairs) to a scale as illustrated in Fig. 1. The scale was calibrated to read directly (in milliradians) the shaft angular displacement. Displacements of 1/2 milliradian could be measured.

Tachometer. An Electrical Indicator Company D-C tachometer was used. Performance characteristics as tested by Mr. D. P. Mason of the Instrumentation Laboratory are presented in Fig. 10. The tachometer was separated from the motor by a gear reduction of 12.82 because of the high friction level in the tachometer. This permitted some signal distortion due to backlash during oscillation, but it was believed to be unimportant. Ripple factor at steady speed was about 0.01. The slope of Fig. 10 is 0.0216 volt per revolution per minute, which with proper unit conversion is 0.207 volt per radian per second.

Velocity signal attenuator. A 5000 ohm variable resistor was used. Attenuation of the tachometer signal was necessary to establish a damping ratio, $\zeta_{(ps)}$, for the servo. The following settings were used based on a specific forward loop gain $S_{(ps)[A;M]}$ of 243 ounce-inches per radian.

Damping ratio	Attenuator
0.05	0 ohms
0.2	0.31K
0.5	0.60K
0.7	1.16K
1.0	1.85K
2.0	3.75K

Velocity signal modifier. The modifier was a high pass R-C filter with a time constant adjustable through variation of resistance. A by-pass was provided. Test input and output jacks were used for setting the time constant. Figures 5 and 20 show the filter modifier, its performance function, and associated frequency response. Values of R and C were chosen so their product RC, which is the time constant of the modifier, would cover the desired range. C was made as large as possible in order that R could be made as small as possible in relation to the resistance in the adder circuit, Figs. 2 and 3. The choice of capacitance is made to minimize possible loading effects on the filter. It turned out not to be possible to eliminate loading effects completely. The implications of loading effects on the test results are discussed in Chapter 5.

Displacement signal modifier. This was a low pass filter or integrator using a Reeves Instrument Company MK 77 Mod O computing d-c amplifier. Figures 2 and 4 show the modifier and Fig. 6 is a wiring diagram of the amplifier. Figure 24 shows the performance function and the associated frequency response. The time constant was altered by varying the 2.5 M ohm variable resistor. A shorting switch was installed across the feedback capacitor to establish zero initial conditions, and a by-pass was provided around the entire unit. Test jacks were used for setting time constants. The open loop gain of the amplifier alone was 10×10^6 to 30×10^6. Even with chopper stabilization the amplifier when connected as a straight amplifier with resistive feedback and a gain of 10 had some zero input offset voltage (about 1 millivolt), and when connected as a straight integrator with 1M ohm input resistor and 0.25 μf capacitance feedback, it has 0.66 millivolt per second output. This indicated that when operating in the modifier circuit some extraneous signal was produced. But since it was in a closed loop, it could only induce some small amplitude, slow speed, motion of the controlled member. This was checked, and no measureable effects were observed within a period of minutes.

Polarad power unit. A Polarad Power Unit, model PT-111-D, serial 150, made by the Electronics Company, provided a regulated source of ±300 volts d-c and 6.3 volts a-c filament voltage. Grounds for all components of the servomechanism were referenced to the ground of this unit.

Servocope. Type SCA-7031A. This unit, manufactured by the Servo Corporation of America, was used for both frequency response testing and for obtaining repetitive step responses displayed on the cathode ray oscilloscope. An output for testing was available as a square wave or a sine wave at frequencies from 0.2 to 20 cycles per second. A synchronization signal was also available, and a phase shift control governing the phase between output signal and synch signal was used to determine phase angle of servo response on the cathode ray oscilloscope during frequency response testing. See Fig. 2 for details of connections.

Cathode Ray Oscilloscope. Type 304-H, serial 4059 made by Allen B. Dumont Laboratory, Inc., was used.

Sanborn Four Channel Recorder.

Simpson Electric Company Ohmmeter, model 260.

Vacuum Tube Voltmeter. Hewett-Packard Model 4000.

All signal leads were shielded with shielding grounded, and a common ground was provided all components.

CHAPTER 4

INVESTIGATION

I. Testing the servomechanism

It was decided to divide the testing of the servomechanism into two functional divisions. First, the basic model (ps)(b) and the velocity signal damping model (ps)(vsd) should be tested to determine whether or not they perform as predicted, i.e. they do in fact respond as the mathematics in Appendix A dictates. For unless this response could be predicted within reasonable experimental tolerances, the response of the (ps)(mvsd) and (ps)(vsd)(mds) models would be meaningless. Second, after establishing the predictability of the first two models, the second two models should be tested and the results compared with those predicted by Lees in (5).

A. Deviations and uncertainties. It was anticipated that deviations from linear performance and uncertainties both in measurement and component performance would present difficulties. The more troublesome sources of these difficulties are known to occur as follows:

1. Torque generator. The nonlinearities of a 2 phase A.C. motor are well known (3, 4, and 7). Reference to Fig. 9 shows these nonlinearities. Normal testing should place the motor between zero and 1000 RPM and at control voltages of from 0.8 volts to 120 volts. This will cause a large change in $S_{(tg)[e;M]}$ and $S_{(tg)[\dot{A};M]}$. Variation in either one, and especially the first, will cause deviation from the assumed second order linear system and some possible uncertainty in results.
2. Gear train. Effects of gear train backlash and variable friction have been studied (3) and Chapter 26, Volume II of (6). With this in view, any measurement of damping ratio is definitely subject to some level of uncertainty. Since testing for $C_{(d)(res)}$ depends directly on a measurement of a damping ratio, the value of $C_{(d)(res)}$ has wide variability. The value of $C_{(d)(res)}$ has little effect on results, but establishing damping ratios is to be important.

3. Damping ratio measurement. It was intended to use the Transient Peak Ratio curves and Damping Ratio charts on pages 257 and 261 of Volume II, (6). To use these, ratios of magnitudes of succeeding oscillatory peaks are required. These peaks do not follow an exact mathematical envelope and hence, the peak ratios calculated are subject to some variability.

4. Time constants. These were to be set by measuring rates of exponential rise or decay on Sanborn recorder paper tape. For any given response, there is an uncertainty in measuring the decay even for well behaved responses.

5. Loading effects. The mathematical derivation of the performance function of the (vsm) filter, Figs. 5 and 20, assumes no output current. If the adder-chopper unit in Fig. 2 draws any appreciable current from the (vsm) filter, the system response will be altered, probably giving one with less damping. A similar discussion applies to the (vsa) potentiometer.

6. Saturation. Both amplifiers, the adder-chopper circuit, and the motor all are subject to saturation, or limiting of output. It was planned to avoid operation in any region where this may occur. In particular, input angle signals were not to be above 150 milliradians and torques not above 900 gm-in. Despite this limitation, all inputs are required to be large enough to mask noise, friction, etc.

A basic assumption was made at the outset. With the system as assembled, it was found that for the range of gain available and the location of the tachometer, a 4 to 4.25 cycles per second natural undamped frequency operation allowed the wide range of damping ratios necessary for testing. The selected value of the undamped natural frequency also allowed angular displacement error signals of 150 milliradians (high enough above friction level, Chapter 26, Volume II of (6)) and input torque signals of 700 gm-inches (large enough to mask sticking effects[4].) Therefore it was assumed that the servo as assembled and operating in this range met the necessary requirements for torque and load as described in Chapter 2.

[4]The friction level in terms of error angle was found to average ±8 mils. Sticking level torques were found to be between 25 and 50 gm-inches. Also see Fig. 15.

Prior to testing, all equipment was allowed a warm-up period, and gear train elements were cleaned and given a light coat of light oil.

B. Basic Positional Servomechanism (ps)(b) and Velocity Signal Damping Positional Servomechanism (ps)(vsd) testing.

1. Tests for equivalent moment of inertia $I_{(cm)(eq)}$ and residual viscous damping coefficient $C_{(d)(res)}$.

By using the auxiliary springs described in Chapter 3 and with motor fields unexcited, a separate system, having its own stiffness (that of the springs), its own damping coefficient ($C_{(d)(res)(cm)}$), and its own moment of inertia ($I_{(cm)(eq)}$ if effect of the springs may be neglected), could be excited by manually offsetting the controlled member and releasing it while recording the decaying exponential on the Sanborn Recorder. Then with an average measurement of $\omega_{(n)(aux)}$ and $\zeta_{(aux)}$ from repeated trials, $I_{(cm)(eq)}$ and $C_{(d)(res)}$ were calculated. See Appendix B-1. The stiffness was calculated using the slope of Fig. 14(a). Reasonable confidence is felt in measuring this slope and $\omega_{(n)(aux)}$, therefore the calculated value of $I_{(cm)(eq)}$ is felt to be within $\pm 5\%$ of true value. The value of $C_{(d)(res)}$ is open to question, since it depends on the measurement of $\zeta_{(aux)}$.

$I_{(cm)(eq)} = .350$ oz-in-sec^2 $\pm 5\%$

$C_{(d)(res)} = .70$ oz-in/radians/sec. $\pm 50\%$

2. Test for servomechanism (ps)(b) stiffness coefficient.

With auxiliary springs disconnected, and the complete servo (ps)(b) assembled and fully operational at 4.0 cycles per second undamped natural frequency, known torques were applied to the controlled member by attaching a weighted pan to the pulley wheel by a string. For several torques, angular displacement of the controlled member and A.C. amplifier output voltage were measured. A plot of the results is presented in Fig. 15. Calculations made in Appendix B-2 based on these results give:

$S_{(tg)[e;M]} = .058$ oz-in/volt

$S_{(a)}S_{(vsc)} = 193$ volts/volt

$S_{(ps)[A;M]} = 243$ oz-in/radian

$S_{(a)}$ and $S_{(vsc)}$ are listed as a product. Chapter 3 gives $S_{(a)}$ = 3000 to 4000 and $S_{(vsc)}$ = .06. Thus their product is about 210. This is on the order of 195. These two component sensitivities always appear in the equations of Appendix A as a product, and therefore the experimental product of 193 will be used. The measured $S_{(tg)[e;M]}$ corresponds very well with the curves in Fig. 9.

3. Frequency response testing of (ps)(b) and (ps)(vsd) models.

With the A.C. amplifier gain set as in B above so as to obtain $S_{(ps)[A;M]}$ = 243 and $n_{(n)(ps)}$ = 4.0 cps, the tachometer signal attenuator was calibrated to give damping ratios $\zeta_{(ps)}$ of 0.2, 0.5, 0.7, 1.0,and 2.0. This was done by breaking the positional feedback loop, offsetting the input potentiometer 150 m.r., and then closing the loop while recording the angular position error voltage (see Fig. 2). Transient peak ratios were measured and ζ was set by TPR curves on pg. 257, Volume II (6) after repeated trial runs. For ζ = 1.0 and 2.0, pg. 261 of Volume II, (6) was used. (The step response that just failed to overshoot was taken for ζ = 1.0 if doubt existed). With damping ratios established, photographs of an increasing step function response were taken for each value of damping ratio on the CRO, by feeding a repetitive square wave from the servoscope into the adder-chopper and synchronizing the CRO so that only the increasing response was displayed. These photographs are shown in Fig. 16. The time scale is based on half the period of the Servoscope square wave frequency (.2 cps), which was found to be as calibrated to within a few percent.

For the frequency response testing for each value of ζ, a sine wave was impressed as described above and the same error signal recorded on the Sanborn recorder. A range of frequencies from 1.2 to 10 cps was covered while insuring that the amplitude of the input signal remained constant. This was done by monitoring this signal on a CRO. Amplitude of response was measured for each frequency and divided by an assumed amplitude $A_{(ref)}$ which made the amplitude ratio at 1.2 cps frequency equal to that which Fig. 19-34, pg 299, Volume II (6), presented for the same nondimensional frequency ratio (using $n_{(n)(ps)}$ = 4.0 cps).[5] This is not strictly correct and is open to some question, but although not correct, any error in assuming this amplitude ratio will not

[5] $A_{(ref)} = A_{(in)}$ if assumed $A_{(ref)}$ gives correct amplitude ratio.

change the general shape of the curves as plotted in Fig. 17. The resonance peaks will remain at an unchanged frequency ratio, and the phase angle is not affected. The possible error in such an assumed amplitude ratio should not be over a few percent for most frequencies. Figure 17 shows the resulting amplitude ratios based on these assumption, and Fig. 18 shows the phase angle. Figure 19 shows the amplitude ratio frequency response for a damping ratio of 0.7 as compared to the predicted response using two different reference frequencies for frequency ratio.

Based on the response data taken for the (ps)(b) and (ps)(vsd) models, certain conclusions can be made. These are discussed at the end of this chapter under the heading "Discussion".

C. Testing the Modified Velocity Signal Damping and Modified Displacement Signal, Velocity Signal Damping Positional Servomechanisms, (ps)(mvsd) and (ps)(vsd)(mds).

The (vsm) and (dsm) modifiers are shown in Figs. 4, 5, 20, and 24, and the (ps)(mvsd) and (ps)(vsd)(mds) models are shown in Figs. 12 and 13. A.C. amplifier gain and thus $S_{(ps)[A;M]}$ remained as in part B. Time constants for the modifiers were based on the ratios used in (5), namely, 0.2, 0.3, 0.5, 0.7, 1.0, and 2.0, which when compared with the 4.0 cps servo ($T_{(n)(ps)} = 0.25$ sec), gave necessary time constants of 0.5, .075, .125, .175, .25, and .5 secs for the modifiers. The modifier time constants were established by putting a D.C. step voltage in the input test jacks of the modifier and recording the output signal at the output jacks on the Sanborn recorder running at a known paper rate. The (vsm) modifier response to a step in is a rising exponential, and the characteristic time was measured as for any first order response. Succeeding runs with trial and error settings of the (vsm) resistor allowed calibration of the resistor to give these time constants. The response of the (dsm) for an input D.C. step voltage is an equal step out superimposed on a ramp out, because for

$$[PF]_{(dsm)[e;e]} = \frac{1 + \tau_d p}{\tau_d p} = \frac{1}{\tau_d p} + 1 = \frac{E_{(out)}}{E_{(in)}} \qquad (17)$$

a step in of $E_{(in)} = \frac{E}{p}$ gives:

$$E_{(out)}(p) = -\frac{E}{\tau_d p^2} + \frac{E}{p} \qquad (18)$$

and the time response to this is

$$E_{(out)} = \frac{E}{\tau_d} t + E\,u(t) \qquad (19)$$

This is the ramp and step. For the ramp, the time constant τ_d can be measured off the tape response by measuring the slope of the ramp, inverting it, and multiplying by the amplitude of the step.

$$\text{slope} = \frac{\tau_d}{E}$$

$$\tau_d = \frac{\tau_d}{E} \; E \tag{20}$$

Repeated trials allowed calibration of the (dsm) modifier. Prior to each run, the feedback capacitor, Fig. 4, was shorted to give zero initial conditions, and the magnitude of the input step voltage was made high enough (60 mv±) to mask any effect of extraneous signals.

Each modifier was thus calibrated. Calibration was made with the modifier feeding into its load. Time constant ratios r_v and r_d are based on $T_{(n)(ps)}$ = 0.25 sec ($n_{(n)(ps)}$ = 4.0 cps).

A frequency response test run was made on the (vsm) and (dsm) modifiers using a time constant for each of 0.25 secs. These responses are shown in Figs. 20 and 24, where they are compared with the responses predicted by the performance equation for these modifiers. The response of the (dsm) was taken while feeding into the adder-chopper circuit. No loading effect was present. But the (vsm) response is that for the isolated filter. Loading reduced this response by 10 to 30 percent. This should reduce the damping ratio to below that value expected. Correlation is evident although in each case the amplitude appears shifted slightly to the right. Such a shift could have been caused by having a slightly smaller time constant set than was expected. This could easily be true in view of the inherent uncertainty in measuring time constants as described earlier.

With the performance of the modifiers established, frequency response tests were made of the (ps)(mvsd) and (ps)(vsd)(mds) servo models for a setting of $\zeta_{(ps)}$ = 0.7 and r = 1.0 ($\tau_d = \tau_v$ = .25 secs). This testing was done as described above for (ps)(vsd) model. The response is shown plotted in Figs. 21a and 25a based on $n_{(ref)}$ = 4.0 cps, and in Figs. 21b and 25b using a different $n_{(ref)}$. For each model, the response to step position input (equivalent to 150 m.r.) is shown for various values of ζ and r in Figs. 23 and 27. These may be compared with the response predicted by Lees (5), which are shown in Figs. 22 and 26. These responses were obtained by impressing a square wave on the adder circuit, feeding the error signal to a CRO, synchronizing its sweep with the square wave, and displaying half the period of the square wave on the CRO. Knowing the square wave frequency thus calibrates the trace in time.

The (ps)(vsd)(mds) model was tested for a step application of torque on the controlled member while the sytem was at rest. 700 gram-inches was used. The error signal was fed to a CRO with a camera installed, the CRO sweeping at a known rate. For zero initial conditions in the (dsm) the feedback capacitor was shorted until an instant before application of torque. Two operators were required, a photographer and one who applied the torque. A second CRO, sweeping at the identical rate and phase, was available as a monitor scope. Prior to the start of a test run, the torque operator was standing by with the required weights in the pan and the pan attached to the controlled member by a slack-less string (but not taut). When he observed the monitor CRO sweep nearing a set point, the photographer opened the camera shutter, and on the set point the torque operator unshorted the capacitor and released the weight. Based on the known sweep speed, the time trace in the CRO could be calibrated. Photographs of these responses, done for various values of $\zeta_{(ps)}$ and r_d are presented in Fig. 28, and may be compared with the predicted response from (5) presented in Fig. 26.

During the test runs on the (ps)(vsd)(mds) model, some difficulty was encountered with the gear train. Prior frequency response testing had caused gear tooth wear and an increase of backlash. The results of this wear are evident in the photographs of Figs. 27 and 28.

A second difficulty became evident after all the testing described had been completed. It was found that the gain of the A.C. amplifier had crept up during the testing. Consequently the undamped natural frequency $n_{(n)(ps)}$ had become 4.25 cps instead of 4.0 cps as observed during the initial testing. A defective first stage tube was discovered and thought to be the cause. Since insufficient time remained in which re-runs could be made, no further testing was done. This increased frequency will cause some additional uncertainty in the experimental values of $\omega_{(n)(ps)}$, $T_{(n)(ps)}$, $\zeta_{(ps)}$, r_v, and r_d as is seen by Eqs. (A-22), (A-23), (A-24), (A-39), and (A-45) in Appendix A. Since the (ps)(vsd)(mds) model tests were run last, probably this effect would be most pronounced in those results.

II. Discussion of Results.

The (ps)(b) and (ps)(vsd) servo models performed as predicted by the equations within reasonable experimental tolerances and with due regard for the major nonlinearities or uncertainties of the motor and gear train. Component and closed loop testing yielded compatable component sensitivities. See Appendix B-1, B-2. These sensitivities when used in the equations (Appendix B-3) gave a value of undamped natural frequency within 1 to 12% of observed value,

and damping ratio values within 10 percent of observed values.[6]

ζ desired	Est. tolerance in measuring	ζ calculated	ζ observed	% difference $\frac{\text{calc-obs}}{\text{calc.}}$
(ps)(b)	40%	.072	.07-.09	3-25%
0.2	20%	.255	0.23	+10%
0.5	20%	.404	0.45	-11%
0.7	10%	.76	0.7	+8%
1.0	20%	1.17	1.1	+6%
2.0	25%	2.31	2.1	+9%

Although the above tolerances were felt to apply to any damping ratio measurement, any damping ratio error on one $S_{(vsa)}$ calibration should be related to the others since calibration was done in sequence. And step function testing was done with large enough amplitudes to minimize the effects of nonlinear friction described in Chapter 26 of Volume II (6).

The step responses of Fig. 16 also bear out this conclusion. Their shape is similar to that of the second order step response in Fig. 19-11, Volume II (6) and their response times (RT) compare favorably:

ζ	$RT/T_{(n)(ps)}$	$RT/T_{(n)}$ based on Fig. 19-9 Volume II (6)
(ps)(b)	5	9
0.2	2	2.2
0.5	1.5	0.85
0.7	1	.45 - .75
1.0	1	.75
2.0	2	1.9

Note: (see comparison of damping ratios of above step responses).

The frequency responses, Figs. 17 and 18 also support this conclusion. They are in general similar to those in Fig. 19-34 and 19-35 of Volume II (6). The fact that the phase angles are not exactly -90 degrees at a frequency ratio of 1 is attributed to the inherent difficulties and inaccuracies in phase angle measurement. Phase angle values too low at higher FR are probably due to delay caused by gear train backlash. For a closer comparison, Fig. 19 shows the amplitude ratio AR plotted against FR for a damping ratio of .7 alone. Two reference

[6]Damping ratios computed by both Response Time (Fig. 19-9, pg. 265 of Volume II of (6)) and TPR (Fig. 19-4, pg. 257, Volume II (6)). RT values used for $\zeta > 1$, and TPR given more credence than RT for $\zeta < 1$.

frequencies are used to nondimensionalize the frequency scale, 4.0 cps as was used in Fig. 18a, and 4.6 cps. The use of 4.6 cps is justified for the following two reasons. First, during testing the natural frequency crept upwards to 4.25 cps, and hence is uncertain but tends toward a value higher than 4.0. Second, in the frequency band below 4.0 cps (FR < 1), amplitude is nearly constant and velocity increases nearly directly with frequency. Near FR = 1, velocity is near its maximum. Above this, amplitude decreases with the square of frequency, and velocity varies inversely with frequency. As described earlier, $S_{(tg)[e;M]}$ varies inversely with velocity. Hence, the actual amplitude response should be lower than the predicted values in the range just below, at, and just above FR = 1, with the most deviation near FR = 1. And because of assuming $A_{(ref)}$ (see frequency response testing of (ps)(vsd) model, this chapter) at n_f = 1.2 cps to give the expected AR at this frequency, $A_{(ref)}$ was probably assumed too small. Had a larger value been chosen, the plotting would have been more in coincidence with the predicted values. Assuming a higher value for reference frequency $n_{(ref)}$ accomplishes the same correction, and in view of both reasons, this was done. Using 4.6 cps causes coincidence on Fig. 19.[7]

Based on the correlation between calculated natural frequency, damping ratios, and stiffness, and observed values, and on step response and frequency response correlation, the (ps)(b) and (ps)(vsd) model is considered as having a predictable response. Therefore when modified with predictable (vsm) and (dsm) modifiers its performance should be predictable, and comparison between this and the responses shown in the design basis under consideration (5) is justified.

The frequency response characteristics of the (vsm) and (dsm) modifiers nearly coincide with response calculated from the respective performance functions. See Figs. 20 and 24. Deviation is only 5 to 10 percent. In each case it appears that the characteristic time was set slightly low. Estimates of the uncertainty involved in measuring these characteristic times are shown below

τ	Percent Tolerance
.05	25%
.075	20%
.125	10%
.175	10%
.25	10%
.50	10%

[7] A value of $n_{(n)(ps)}$ = 4.6 cps can be obtained using $S_{(tg)[e;M]}$ = .07 oz-in/volt. This sensitivity is possible. See Appendix B-2 and Fig. 9.

It appears that the (vsm) modifier will pass slightly less damping signal than expected for this one calibration, thus reducing the expected damping ratio, and that the (dsm) modifier will produce a stiffer system than predicted. Since the (vsm) modifier suffered loading effects, this too should tend to reduce damping. But since deviation was shown small, both units are taken as performing properly and the servo models incorporating these modifiers merit some confidence as a basis for comparison.

Figures 21a and 25a show how the frequency response of the (ps)(mvsd) and (ps)(vsd)(mds) models compares with that of the performance functions for one damping ratio and time constant ratio. The deviation noted, most probably, can be explained by the same argument given for choosing a different reference frequency for the (ps)(vsd) model frequency response. Figures 21b and 25b show much more correlation when 4.6 cps is used as reference frequency. Additional weight is given to this argument for the (ps)(vsd)(mds) model since the (dsm) modifier was shown to pass more signal than expected. In Fig. 21a for the (ps)(mvsd) model, the high frequency slope appears that it may approach theoretical as an asymptote.[8] If this is the case, then a good argument prevails for correlation, since this would indicate a system with nearly the same undamped natural frequency but a smaller damping ratio.[9] Due to the number of uncertainties involved, the reason for the deviation cannot be fully explained with the information at hand. However, since the response is in general the same as the theoretical and because a higher than expected amplitude ratio was also obtained for the unmodified system, Fig. 19, the performance of both modified models within experimental tolerance is judged to be that predicted by the design basis.

The step responses for both (ps)(mvsd) and (ps)(vsd)(mds) models (Figs. 23 and 27) bear a marked resemblance to those predicted (Figs. 22 and 26) for the models by Lees. The general trend of response as damping ratio and time constant ratio change is markedly similar. Instabilities occurred almost as predicted. Actual response is somewhat less oscillatory in the lower time constant ratio range, but the difference does not exceed that which might be expected from the uncertainties discussed earlier. Tables I, II, and III compare certain actual and redicted measurements for the two models. Response time is taken as the number of (ps)(b) undamped natural periods $T_{(n)(ps)}$ required for the

[8]Same observation applies for (ps)(vsd)(mds) response in Fig. 25b.

[9]A smaller damping ratio is possible when (vsm) loading of 10 to 30% is taken into account. But due to an increase in $S_{(tg)[\dot{A};M]}$ and a decrease in $S_{(tg)[e;M]}$ with velocity, a higher damping ratio than expected is possible.

response to come within and remain within five percent of final steady state value. This data was taken from measurements made on CRO photographs and, as such, can be no more than an estimate.

It has been shown that within the limits of the nonlinearities and uncertainties discussed, the basic and velocity signal damping positional servomechanisms had a predictable performance, that the velocity signal and displacement signal modifiers also had predictable performance. And the responses of the modified velocity signal damping and velocity signal damping, modified displacement signal positional servomechanisms compared with those predicted by Lees in his design basis. Based on these results, it is considered that for these two modifications the design basis has been substantiated. Experimental verification thus has been obtained.

CHAPTER 5

CONCLUSIONS AND RECOMMENDATIONS

In order to verify the experimental design basis suggested by Lees, a basic and a velocity signal damping position servomechanism was built and tested and found to have a response which was predictable from its associated mathematical equations. Velocity signal and displacement signals modifiers were also constructed and tested and found to have predictable performance. When these modifiers were incorporated in the basic servomechanism, the servo as modified responded to certain inputs as predicted by the design basis. Major uncertainties and nonlinearities have been taken into account. The design basis has been experimentally verified for the two modified models tested.

The servomechanism used for testing can be classed as an instrument servomechanism. As such, it might be considered an analogue computer in itself and the performance obtained thus another computed response. This is true to some extent although certain nonlinearities and delays do in fact exist in the servomechanism discussed. Perhaps had larger or more complex components been used in the test machine, or had a hydraulic instead of an electrical system been used, correlation between predicted and actual response might not have been so close.

With the responses predicted by the design basis at hand, the designer may immediately select the approximate parameters for the system under study and with this advantage devote his time to further refinement of this initial selection. Or several alternate modifications might be compared during this phase by reference to the design basis, if the design basis were expanded to include any number of the modifications possible in this field.

It is suggested that further study of other possible modifications be included in the design basis. It is recommended that those models now included therein which were not verified during this investigation and whatever other models as are studied at a later date be verified by similar or other experimental means.

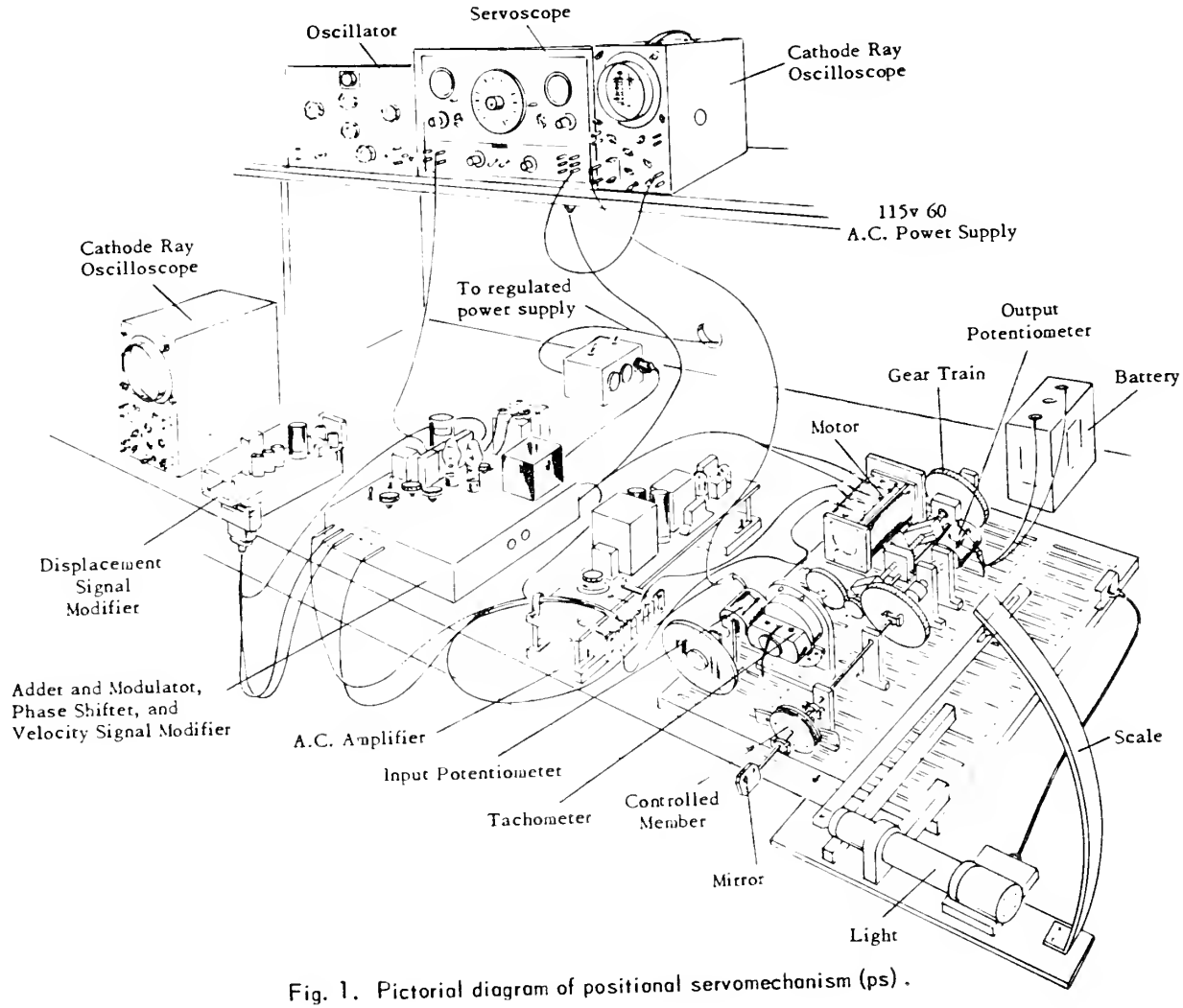

Fig. 1. Pictorial diagram of positional servomechanism (ps).

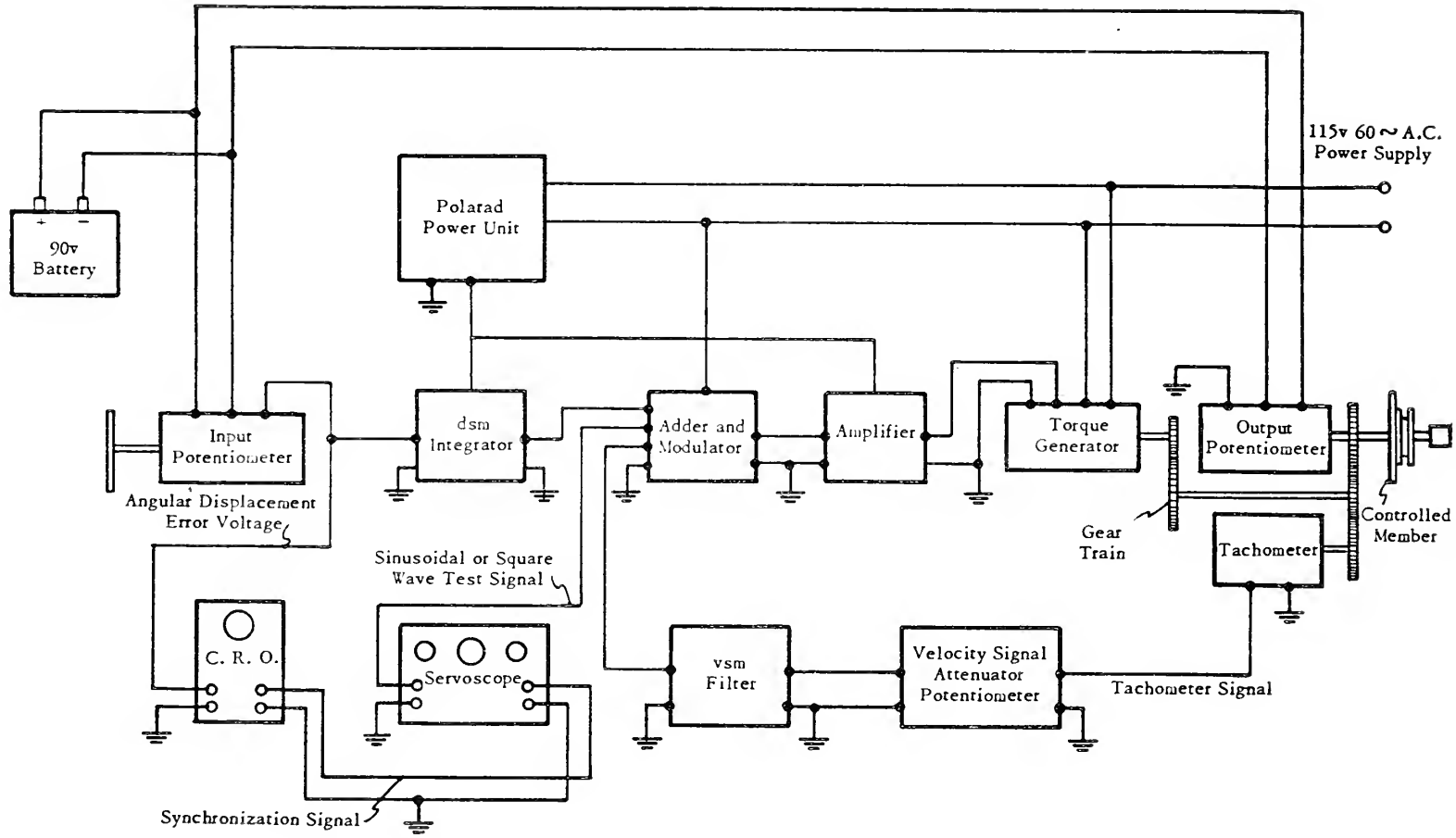

Fig. 2. Functional diagram of positional servomechanism (ps), including modifying components.

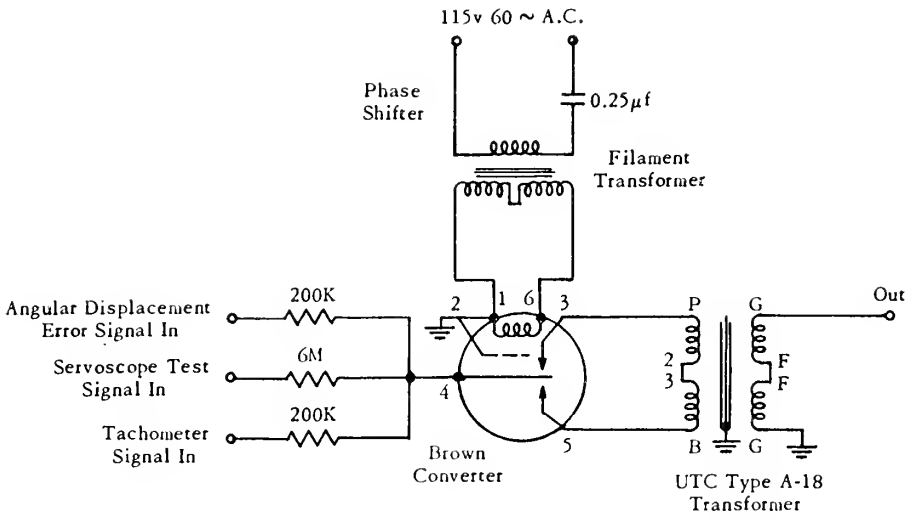

Fig. 3. Adder and modulator.

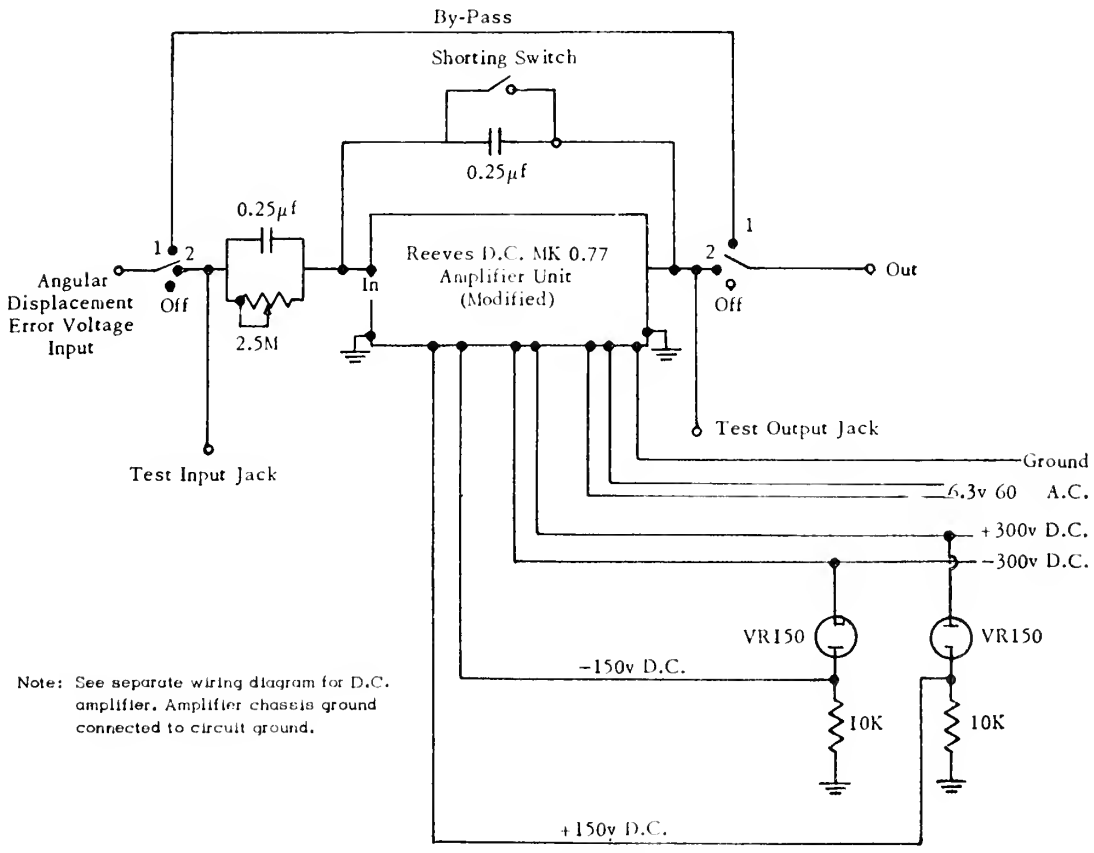

Fig. 4. Displacement signal modifier (dsm).

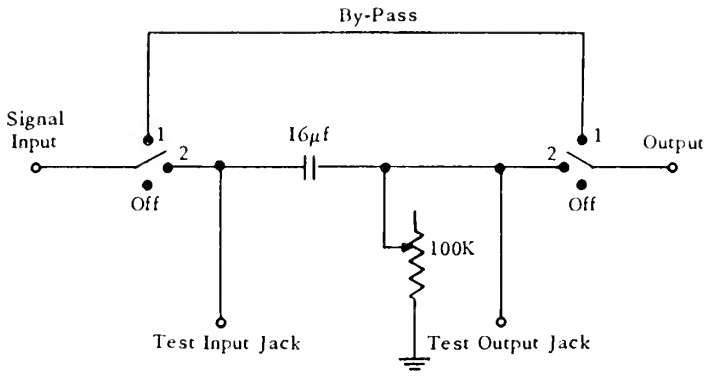

Fig. 5. Velocity signal modifier (vsm).

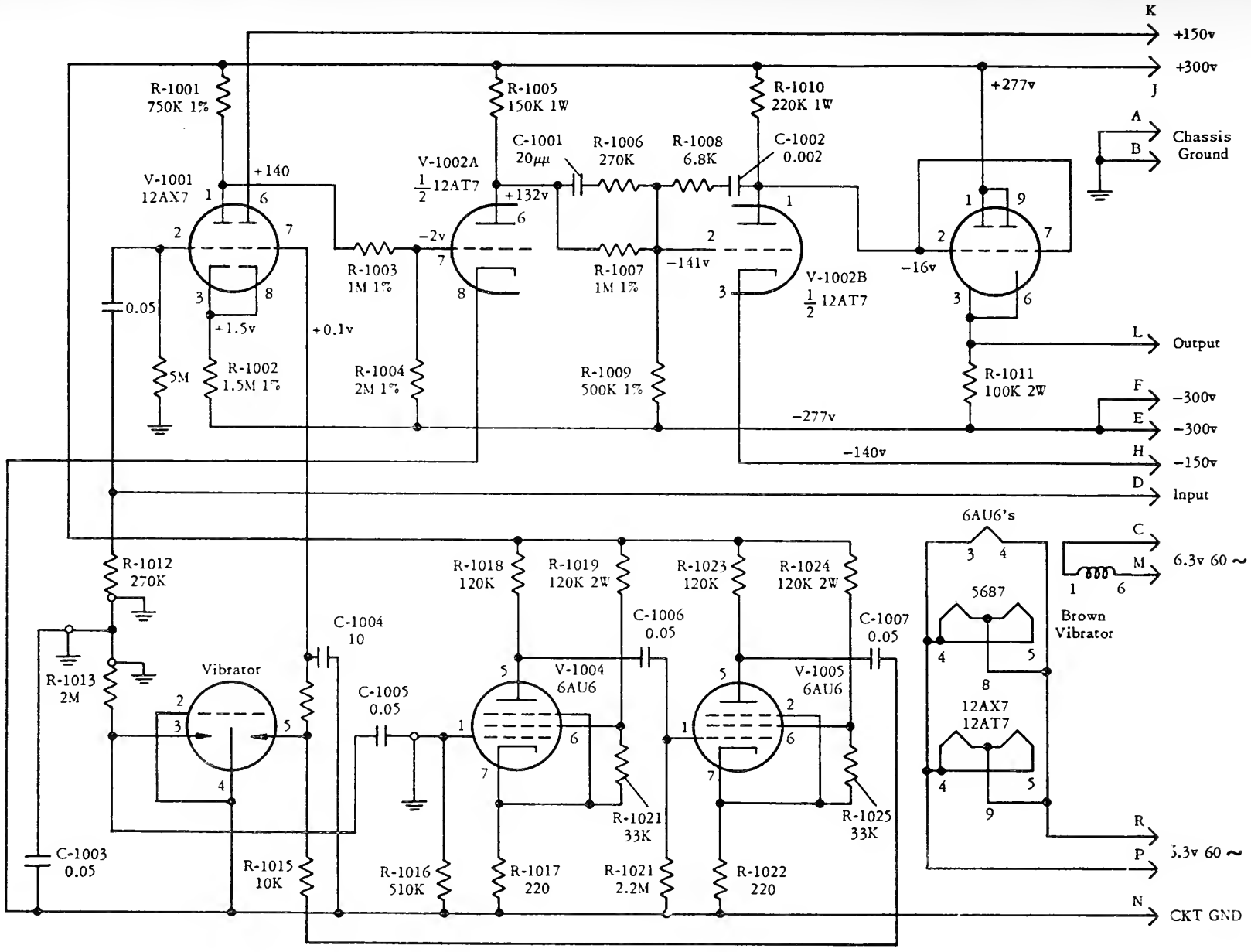

Fig. 6. Reeves D.C. amplifier MK77 MOD 0 wiring diagram.

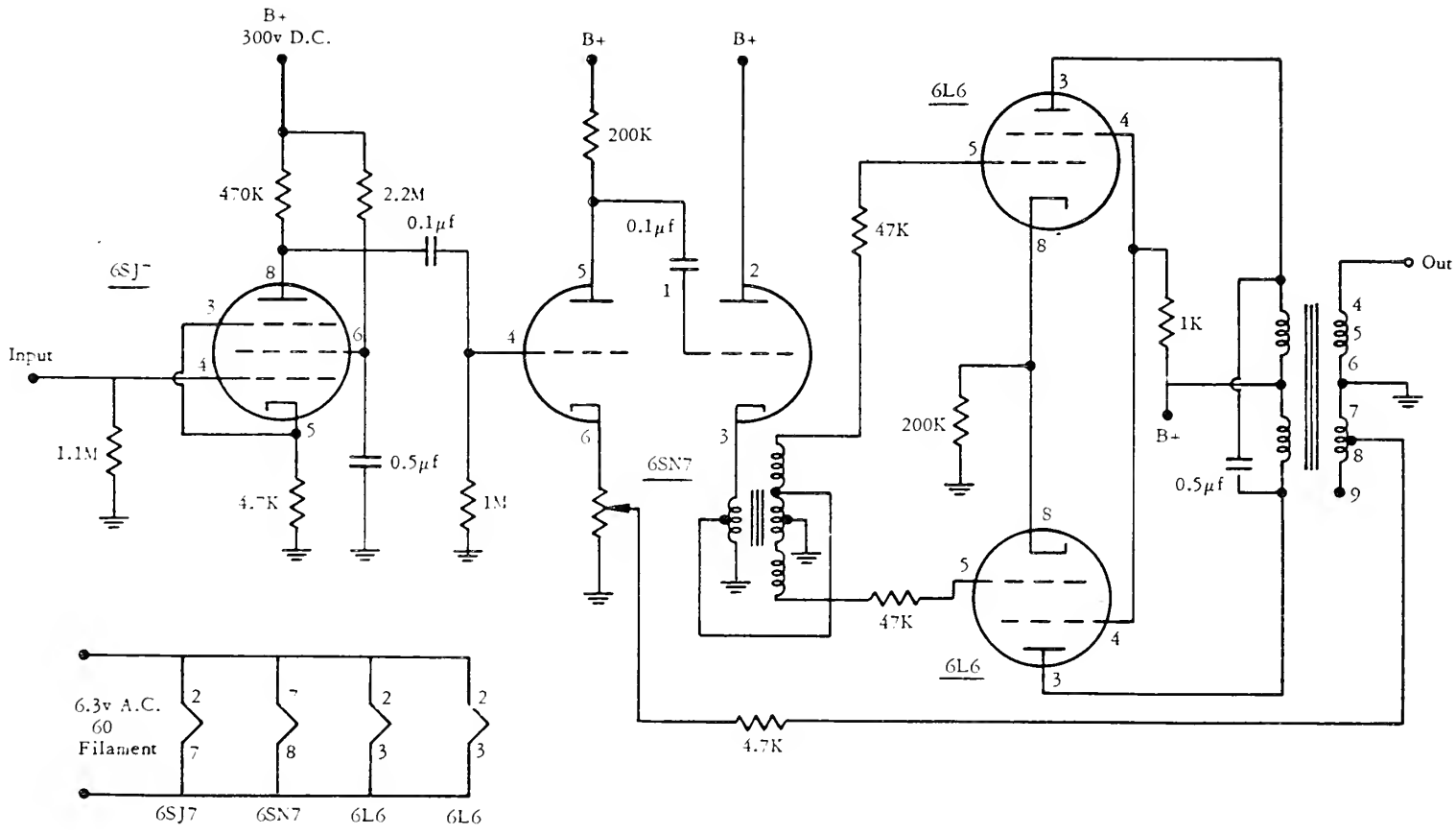

Fig. 7. Reeves A.C. amplifier wiring diagram.

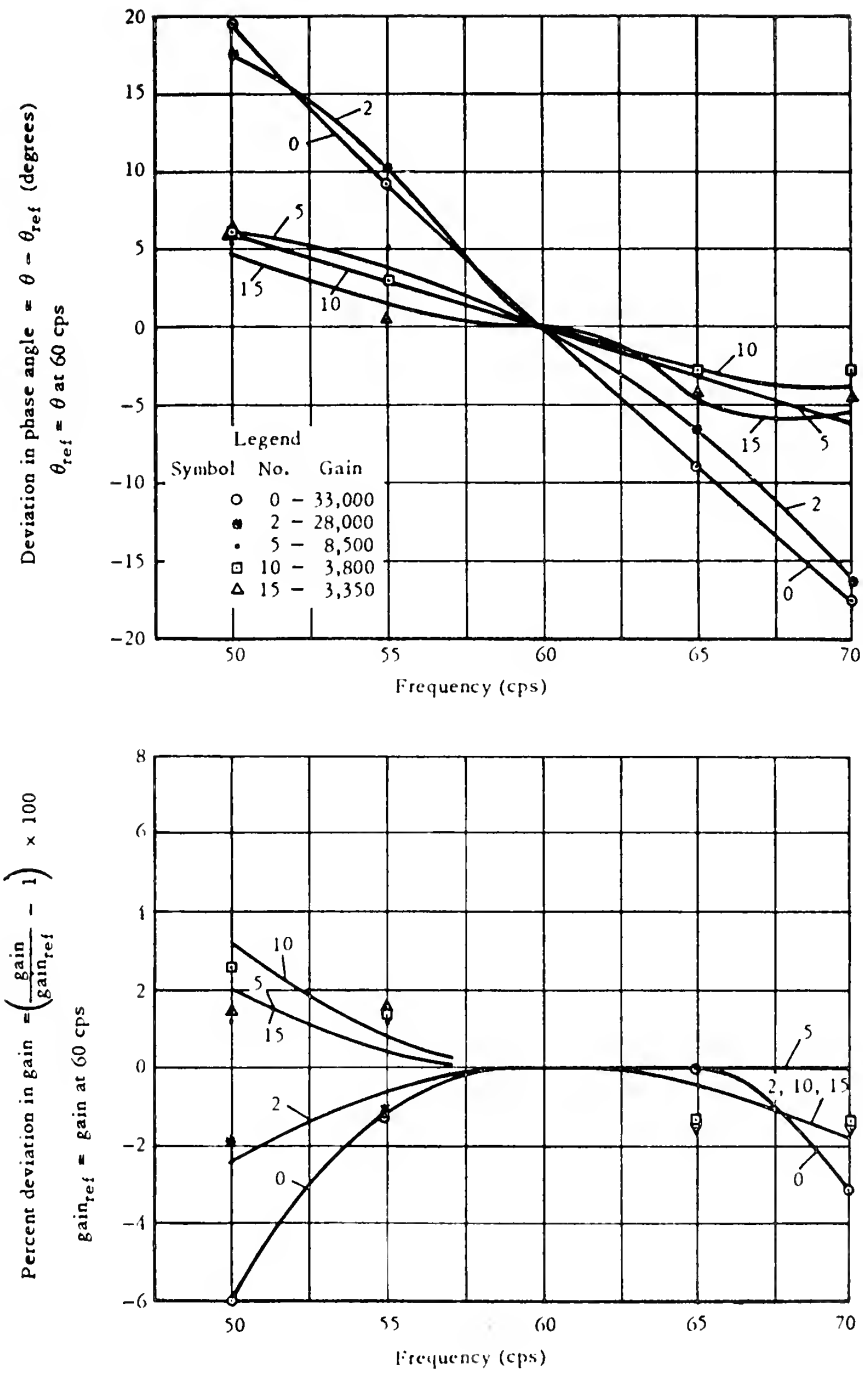

Fig. 8(a). Deviation in A.C. amplifier gain and deviation in phase angle vs frequency (carrier frequency = 60 cps) for various gains.

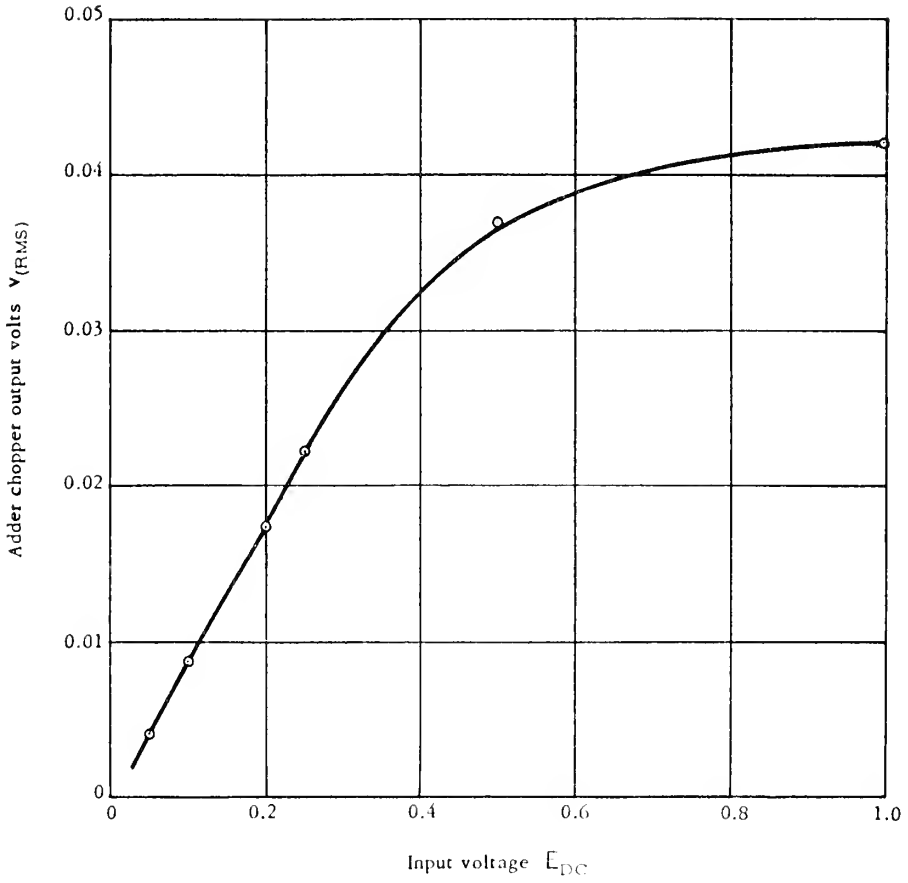

Fig. 8(b). Output voltage vs input voltage for the adder-chopper circuit.

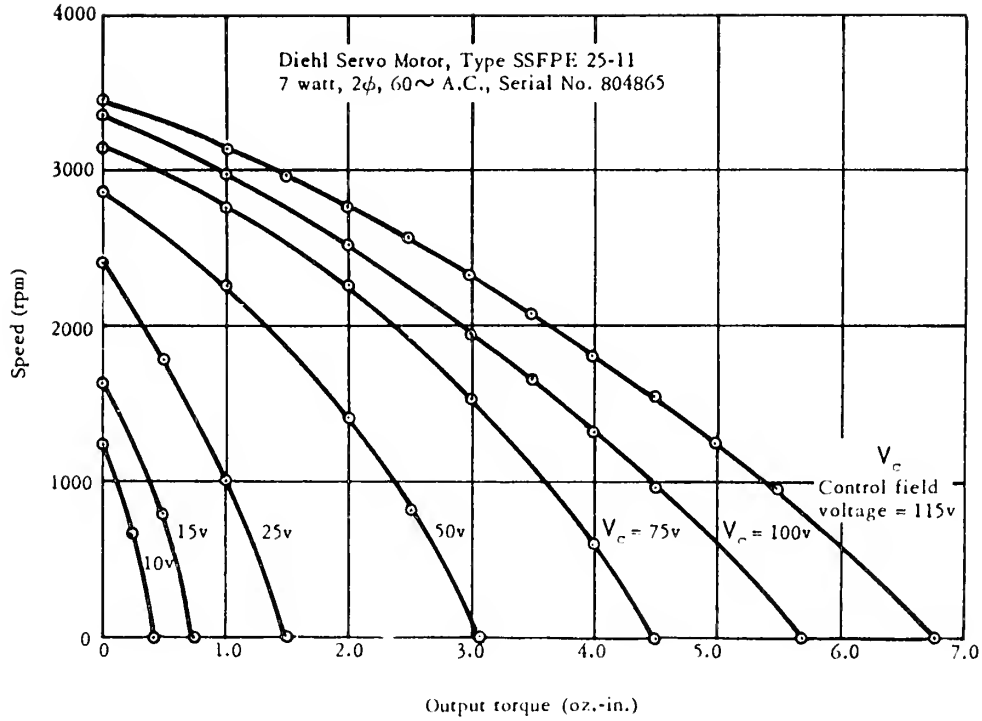

115v 60 cps applied to reference phase
Adjustable voltage applied to control phase

With 115v 60 cps applied to reference phase, motor starts with approximately 0.8v applied to control phase

Fig. 9. Motor characteristics.

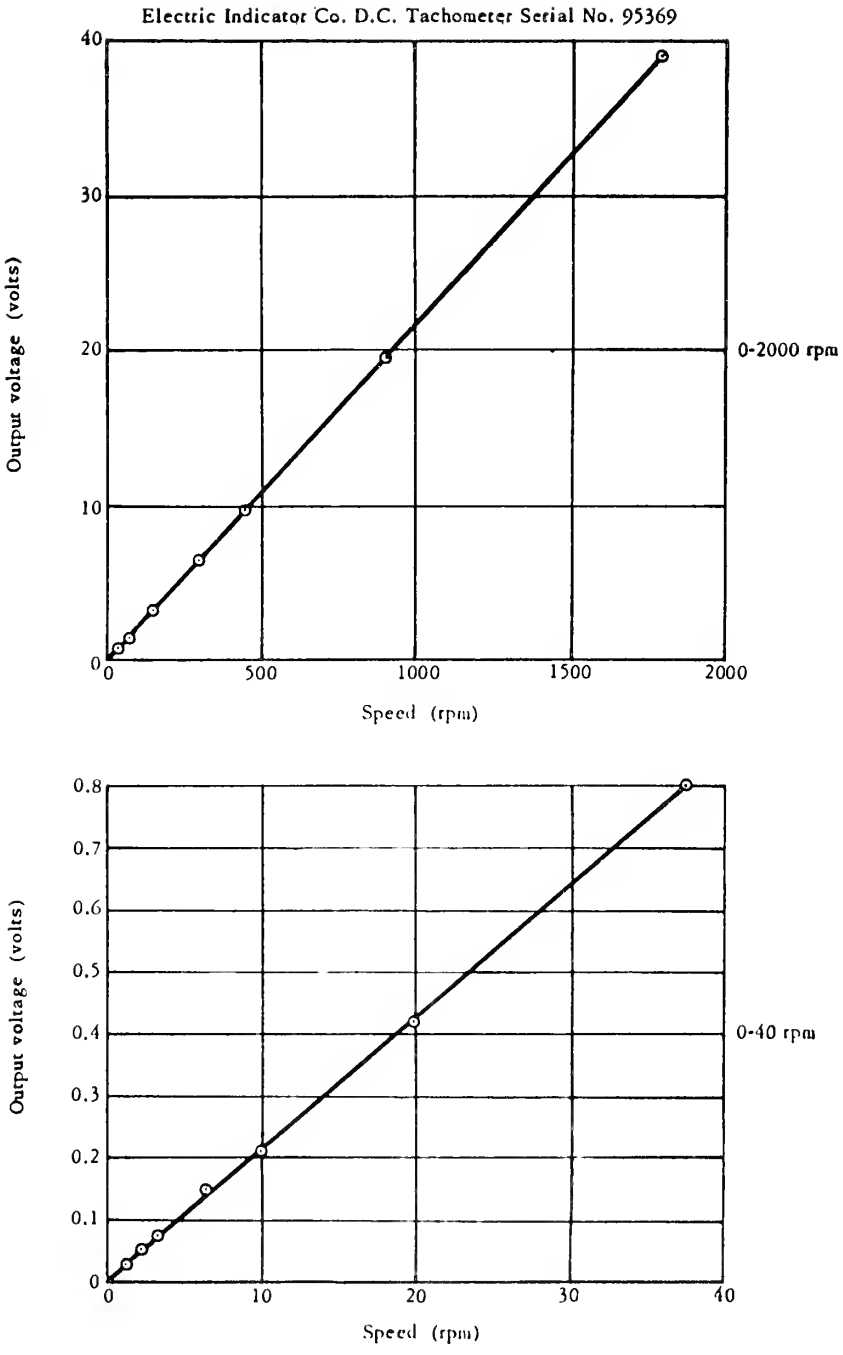

Fig. 10. Tachometer characteristics.

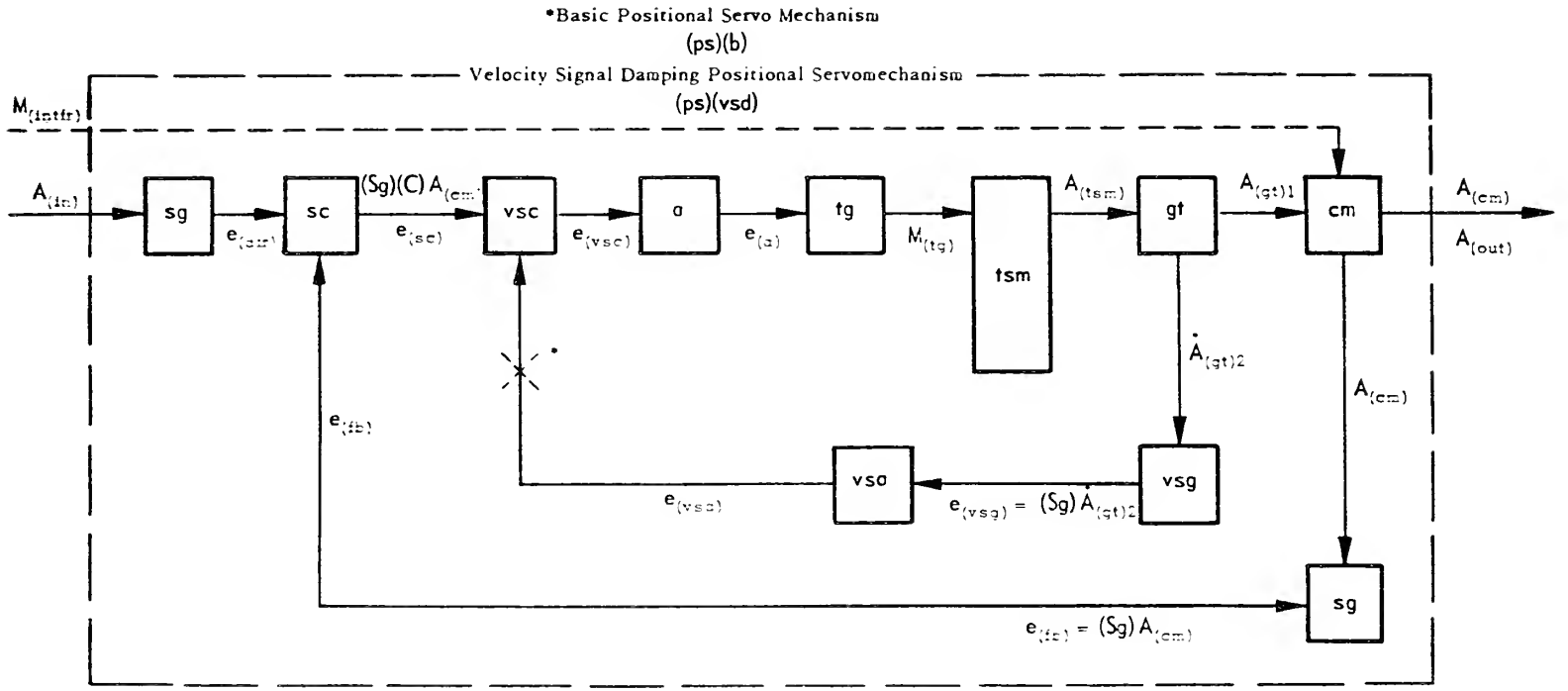

$A_{(in)}$ = input angle
(sg) = signal generator
(a) = amplifier
(tsm) = torque summing member
(tg) = torque generator
(cm) = controlled member
$A_{(cm)}$ = controlled member angle
(sc) = signal comparator
(vsc) = velocity signal comparator (Adder-chopper circuit)
(vsg) = velocity signal generator
(vso) = velocity signal attenuator
(gt) = gear train

$(C)A_{(cm)} = A_{(in)} - A_{(cm)}$
= controlled member correction
$e_{(air)} = (Sg)A_{(in)}$
= input angle signal = direct voltage
$e_{(fc)} = (Sg)A_{(cm)}$
= controlled member signal
= feedback voltage
$e_{(sc)} = (Sg)(C)A_{(cm)}$
= correction signal
$e_{(vsg)} = (Sg)\dot{A}_{(gt)2}$
= torque summing member velocity signal
$e_{(vso)}$ = velocity signal attenuator voltage

$e_{(vsc)}$ = velocity signal comparator voltage
$e_{(a)}$ = amplifier output voltage
$M_{(tg)}$ = torque generator output torque
$M_{(intfr)}$ = interference torque
$A_{(tsm)}$ = torque summing member angle
$A_{(gt)1}$ = gear train output angle to controlled member
$\dot{A}_{(gt)2}$ = gear train output velocity to velocity signal generator

Note: Diagram is for (ps)(vsd) model. For (ps)(b) model, open inner feedback loop at marked *.

Fig. 11. Torque summation functional diagram for basic positional servomechanism (ps)(b), and velocity signal damping positional servomechanism (ps)(vsd).

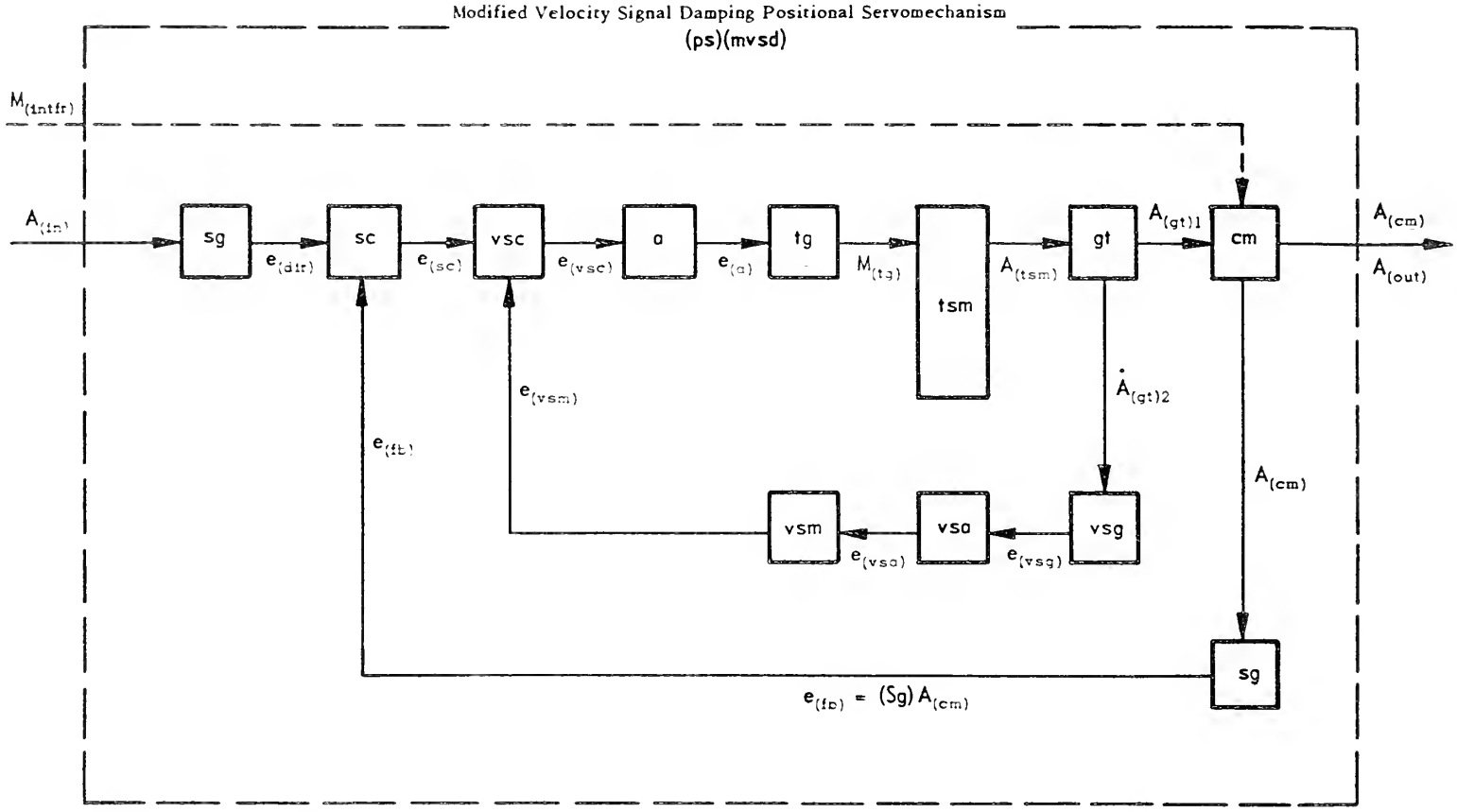

(vsm) = velocity signal modifier

$e_{(vsm)}$ = velocity signal modifier output voltage

For other symbols see preceding figure.

Fig. 12. Torque summation functional diagram for modified velocity signal damping positional servomechanism (ps)(mvsd).

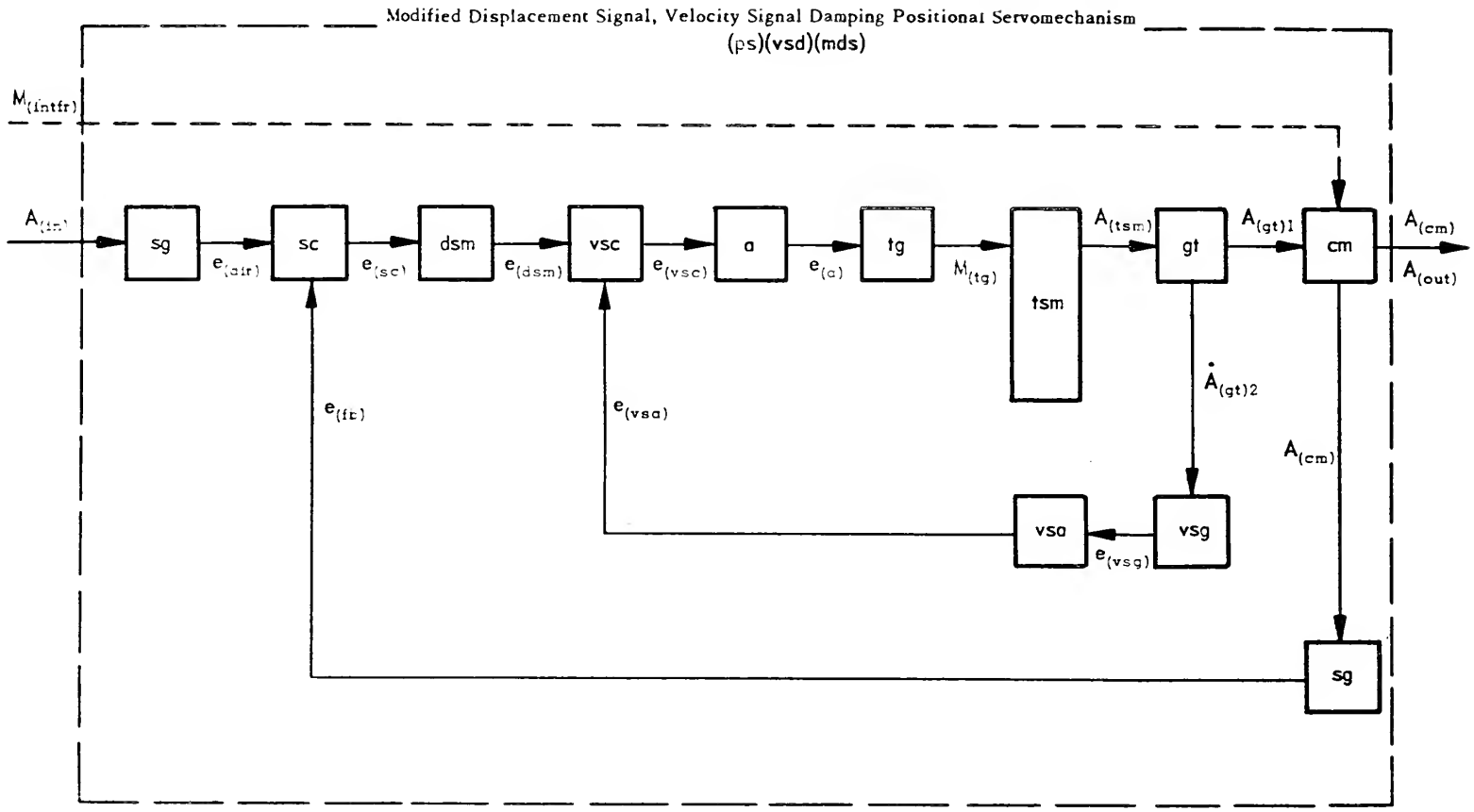

(dsm) = displacement signal modifier

$e_{(dsm)}$ = displacement signal modifier output voltage

For other symbols see preceding figures.

Fig 13. Torque summation functional diagram for modified displacement signal, velocity signal damping positional servomechanism (ps)(vsd)(mds).

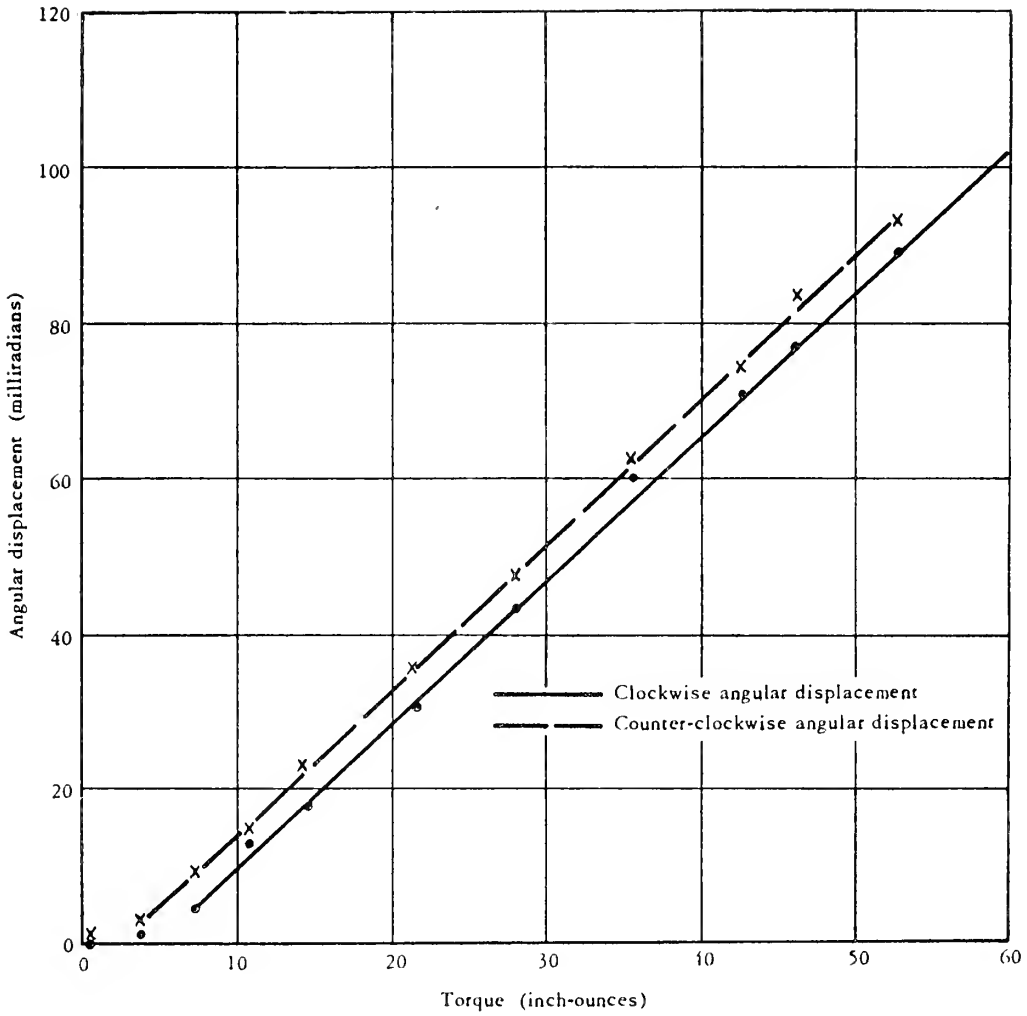

Fig. 14(a). Angular displacement of controlled member vs applied torque (with auxiliary springs attached and motor inoperative) for determination of moment of inertia.

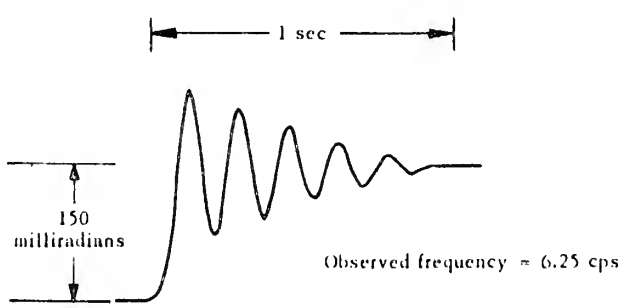

Fig. 14(b). Response of system with auxiliary springs attached and motor inoperative. Angular displacement vs time for a step function input for determination of moment of inertia.

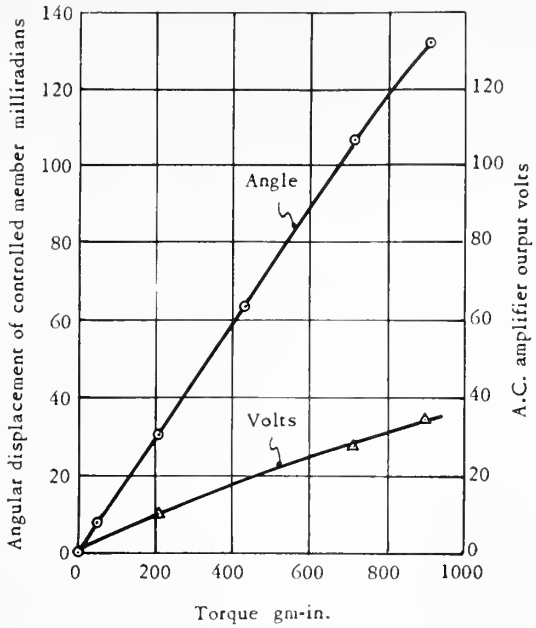

Fig. 15. Static test. Angular displacement of controlled member and amplifier voltage vs static torque load on controlled member.

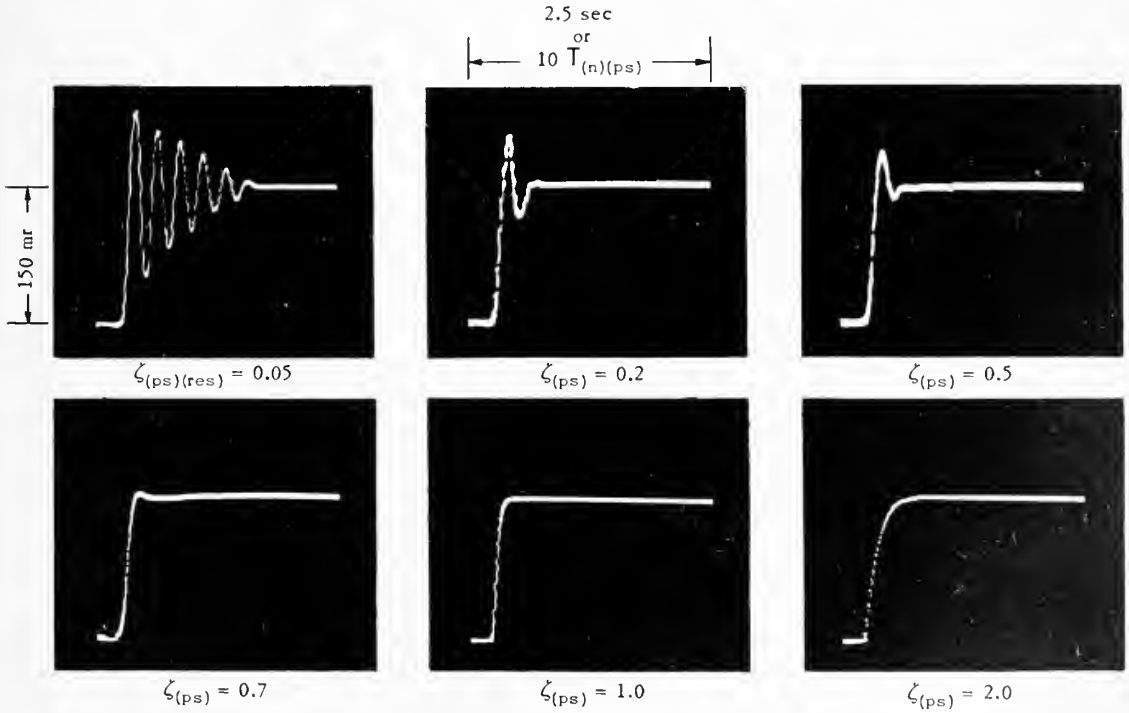

Fig. 16. Increasing step function response of positional servomechanism (ps) and velocity signal damping positional servomechanism (ps)(vsd) for various damping ratios ($\zeta_{(ps)}$). Cathode Ray Oscilloscope photographs of actual responses.

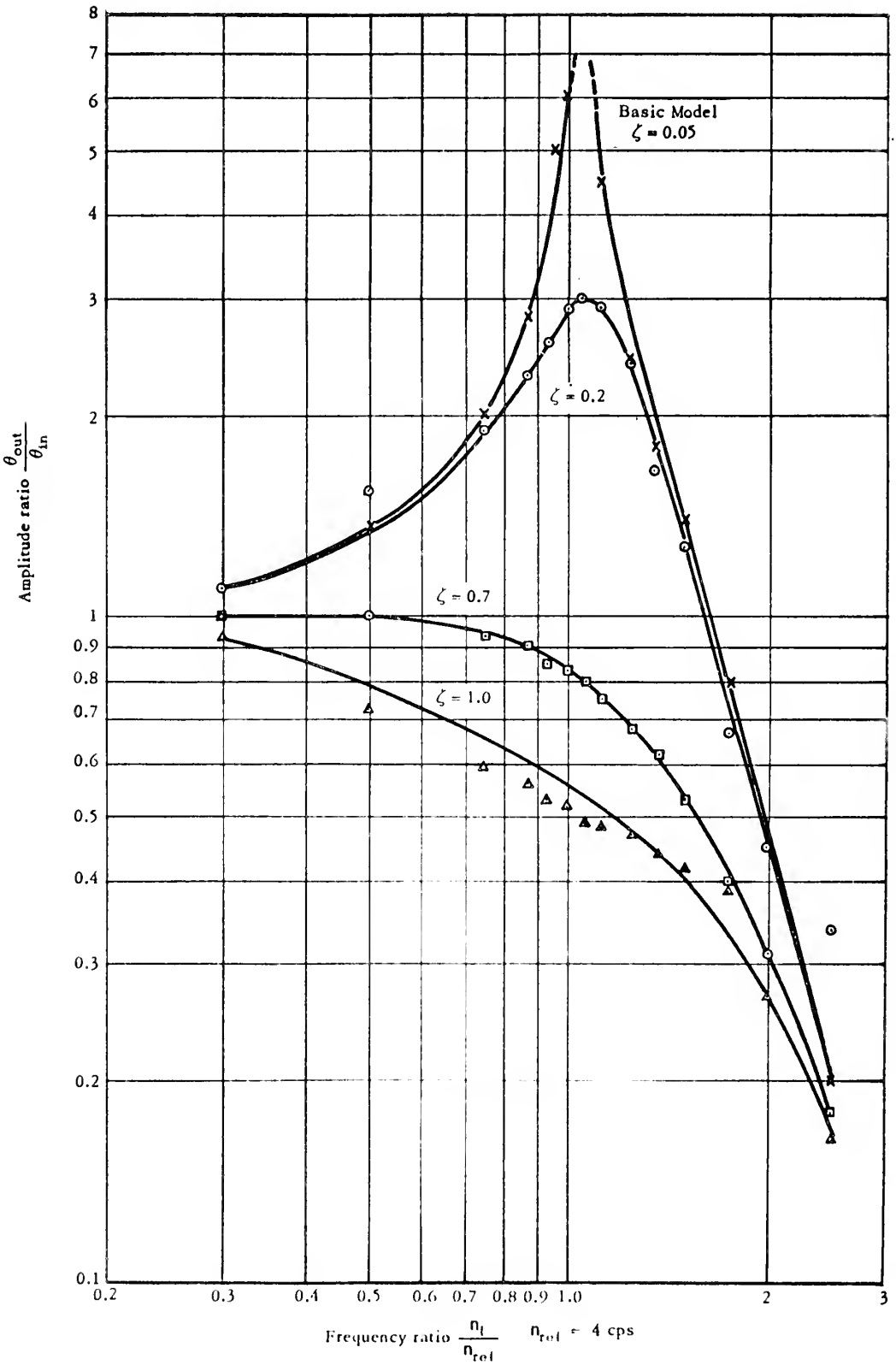

Fig. 17. Frequency response plot. Amplitude ratio vs frequency ratio for basic positional servomechanism (ps)(b) and velocity signal damping positional servomechanism (ps)(vsd).

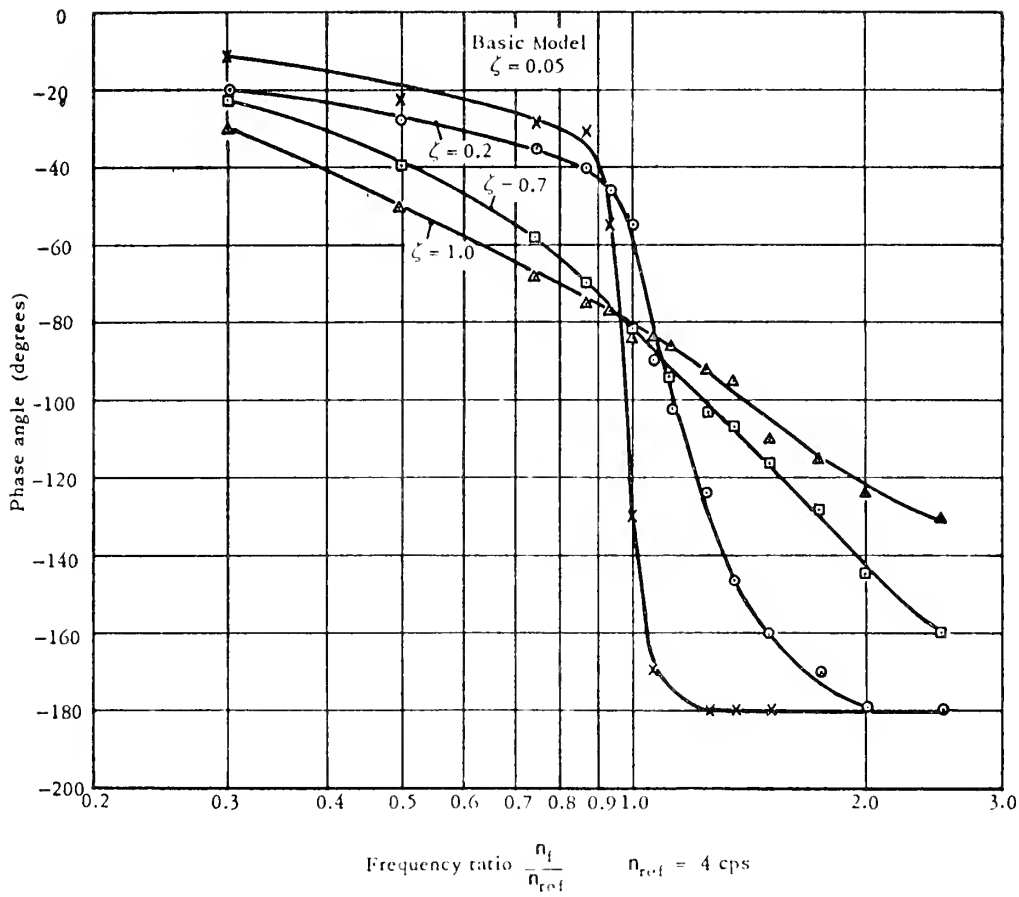

Fig. 18. Frequency response plot. Phase angle vs frequency ratio for basic positional servomechanism (ps)(b) and velocity signal damping positional servomechanism (ps)(vsd).

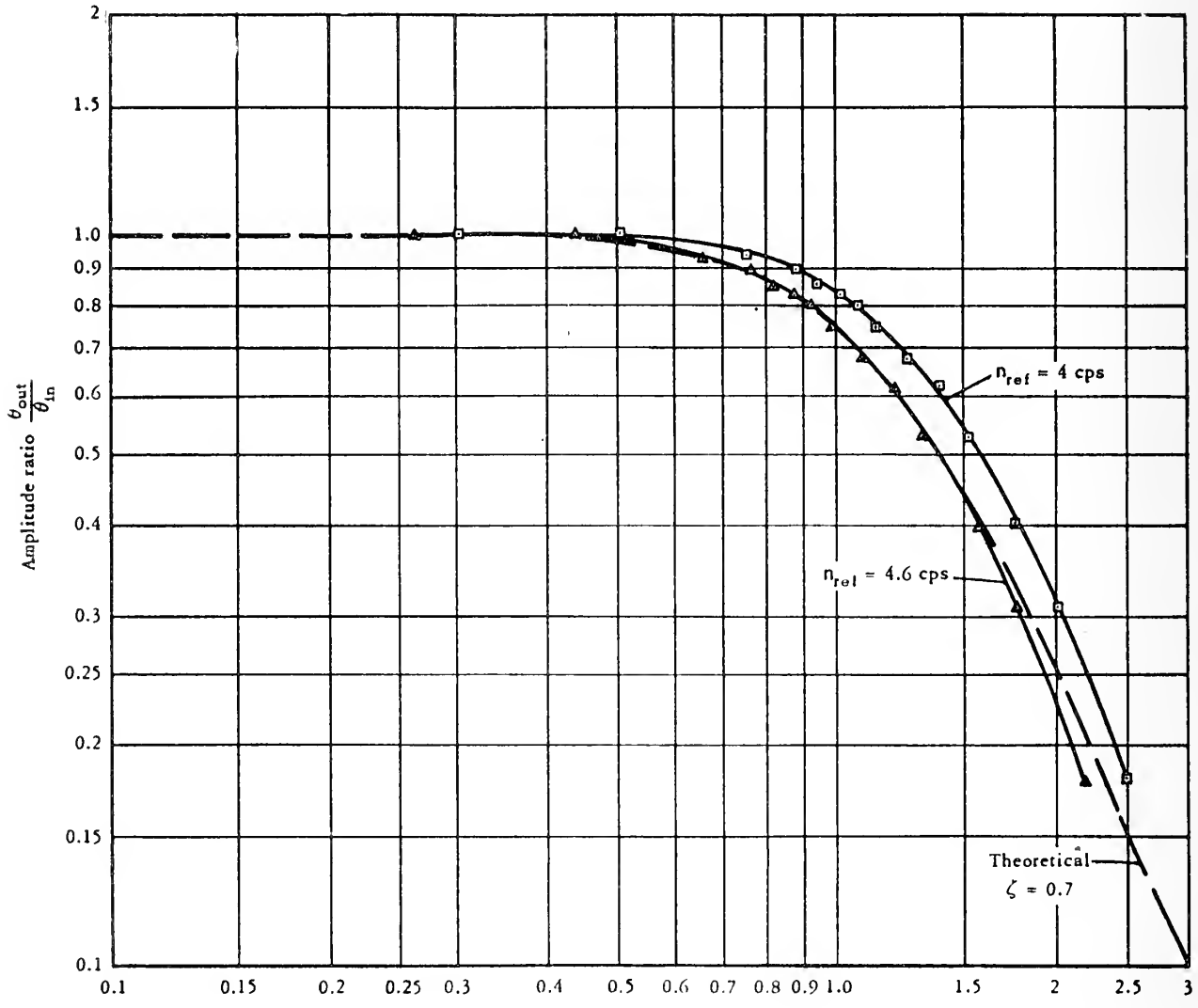

$$[PF]_{(ps)[\Lambda;A]} = \frac{1}{\Lambda p^2 + (2\zeta_{(ps)} + 2\zeta_{(ps)(res)})\Lambda p + 1}$$

Fig. 19. Frequency response plot amplitude ratio vs frequency ratio for velocity signal damping positional servomechanism (ps)(vsd). Damping ratio $\zeta_{(ps)} = 0.7$, showing comparison of results using two reference frequencies n_{ref}.

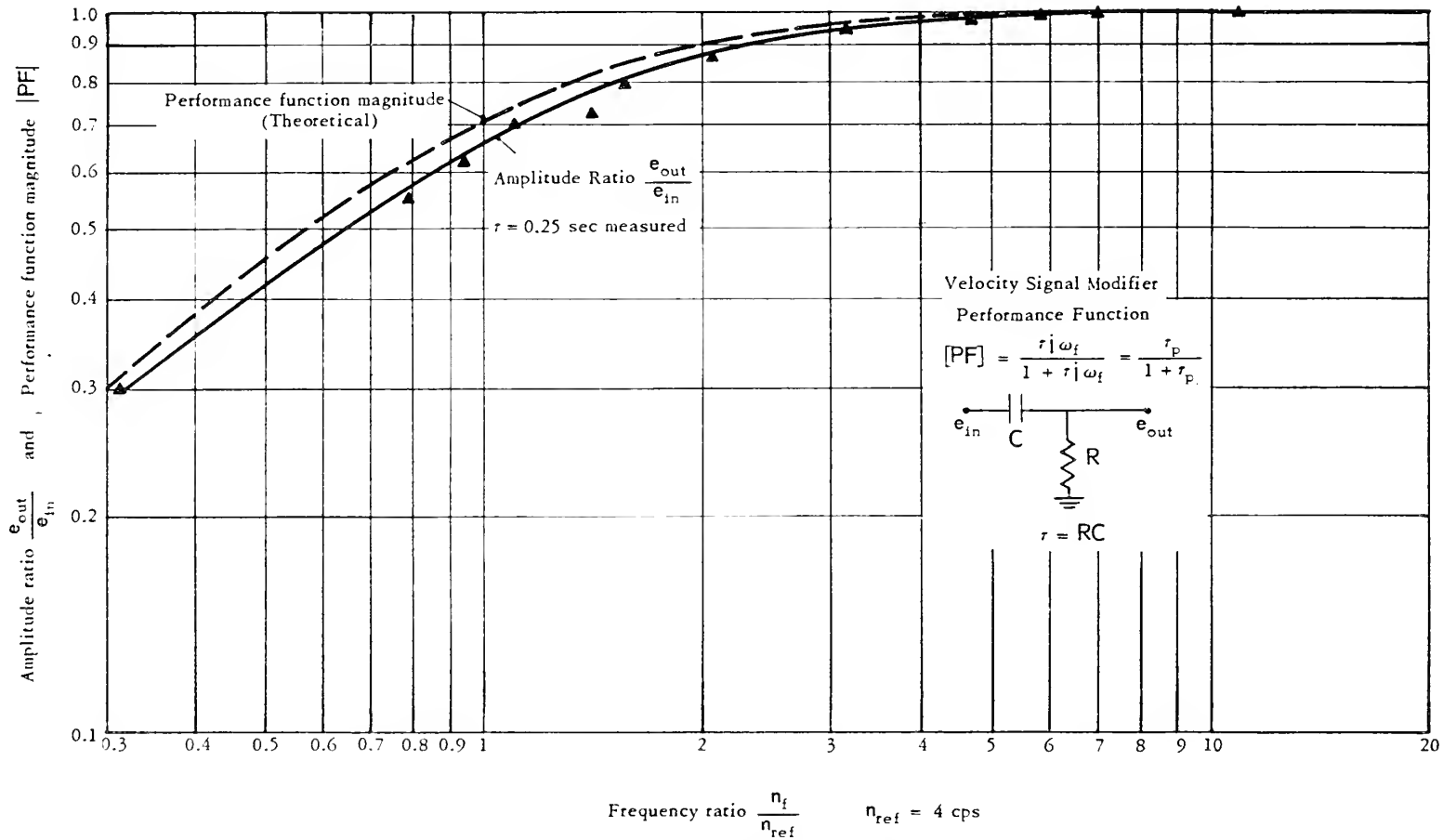

Fig. 20. Frequency response plot showing comparison of predicted and actual responses of the velocity signal modifier (vsm).

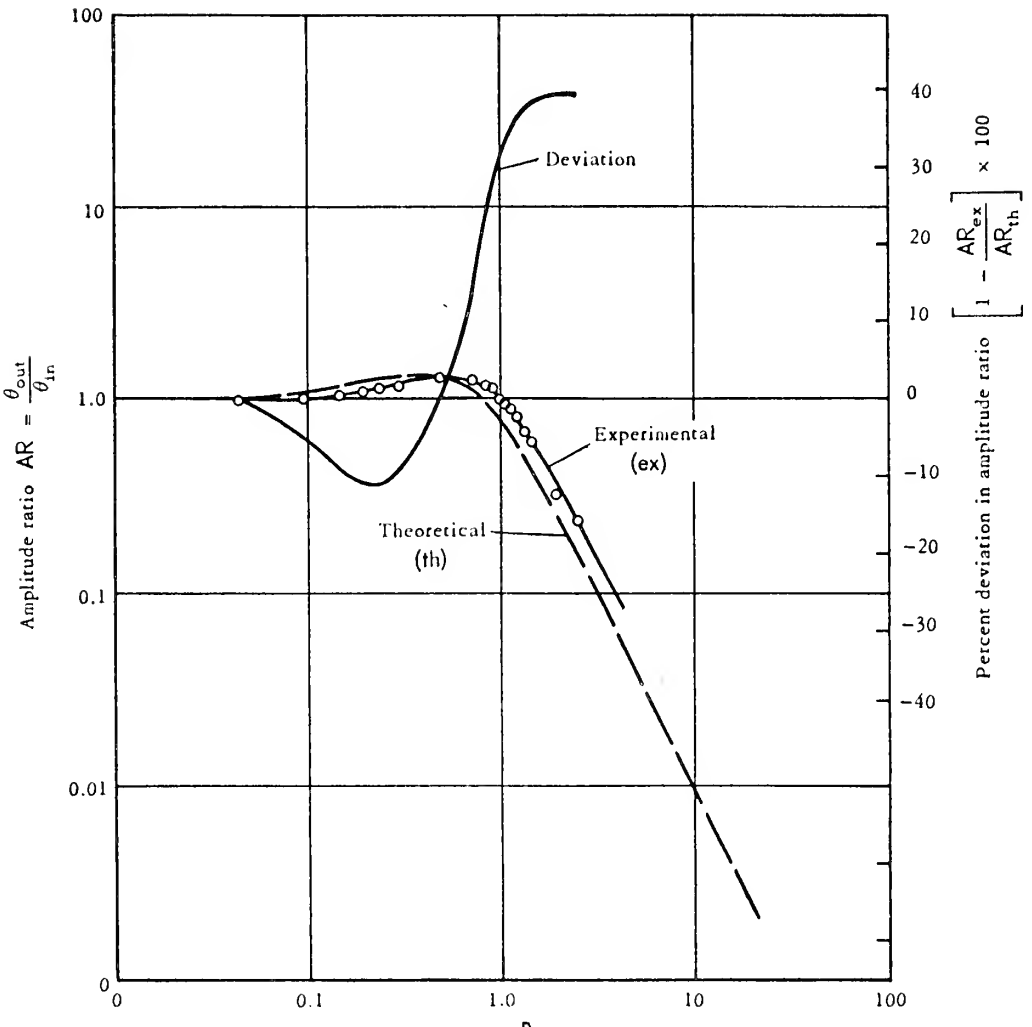

$$[PF]_{(ps)(mvsd)[AA]} = \frac{1}{'p^2 + \left(\frac{2\zeta_{(ps)} r_v 2\pi 'p}{1 + r_v 2\pi 'p} + 2\zeta_{(res)}\right) 'p + 1}$$

$$'p = \frac{p}{\omega_n}$$

$r_v = 0.25$ sec , $r_v = 1.0$, $\zeta_{(ps)} = 0.7$

Fig. 21(a). Frequency response plot amplitude ratio vs frequency ratio for modified velocity signal damping positional servomechanism (ps)(mvsd).

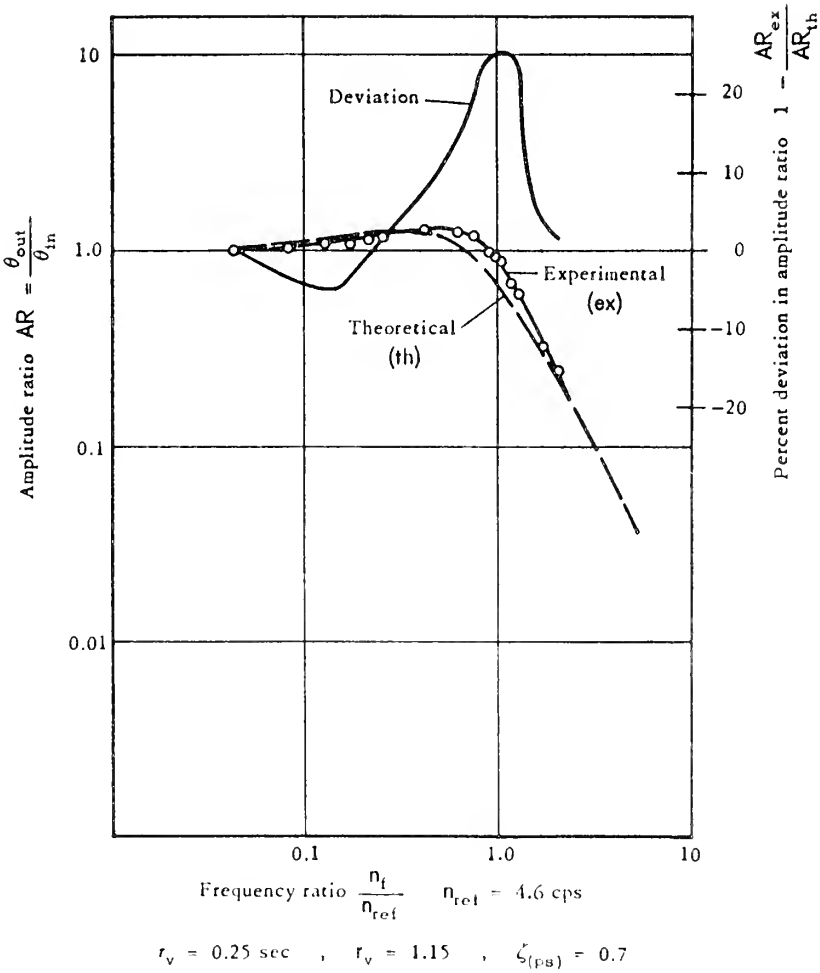

Fig. 21(b). Frequency response plot amplitude ratio vs frequency ratio for modified velocity signal damping positional servomechanism (ps)(mvsd), showing comparison of predicted and actual response when corrected for $n_{n(ps)}$.

Sidney Lees

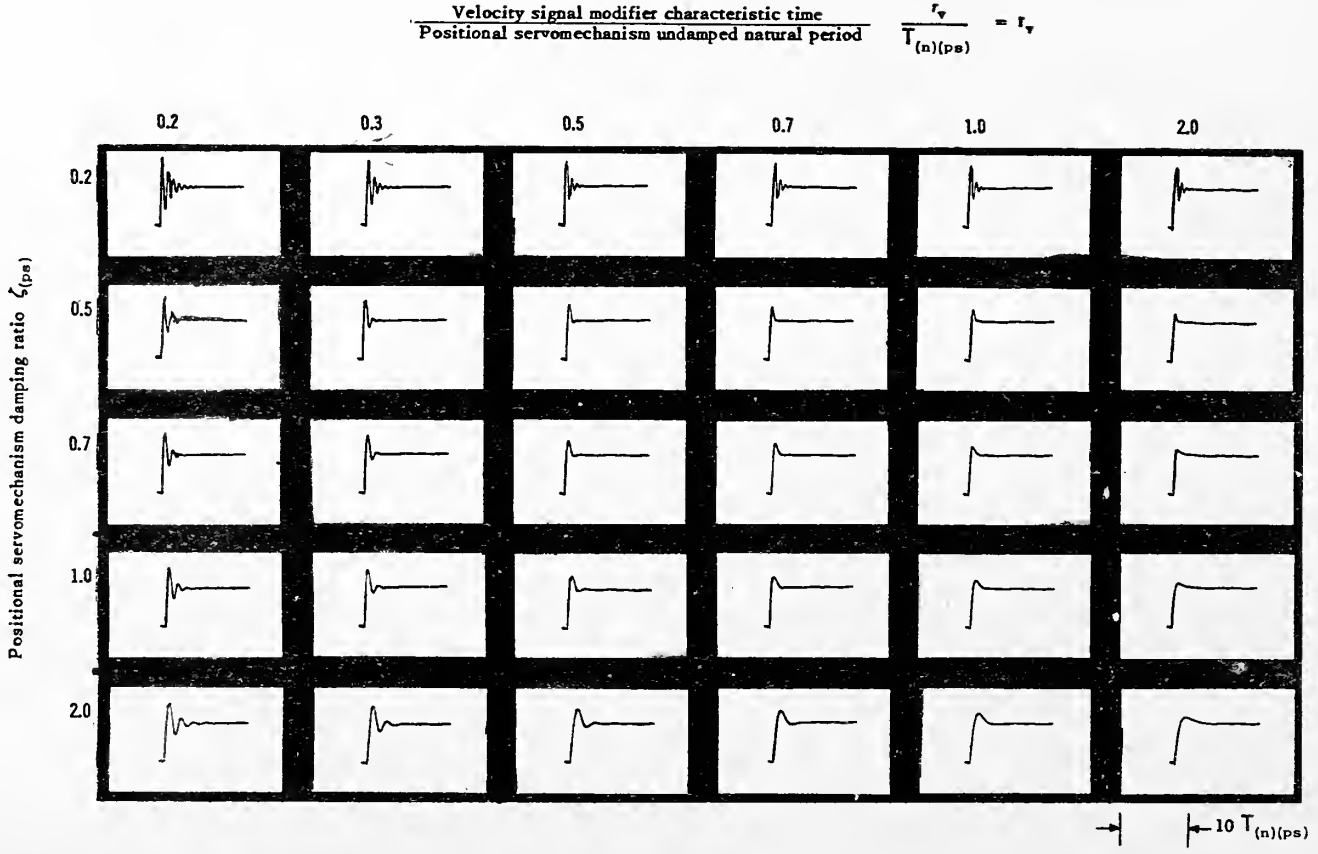

Reproduced from Massachusetts Institute of Technology Instrumentation Laboratory Report R-96 by Sidney Lees, December 1955, by courtesy of Professor Sidney Lees.

Fig. 22. Increasing step function responses of modified velocity signal damping positional servomechanism (ps)(mvsd) for various damping ratios ($\zeta_{(ps)}$) and various velocity signal modifier characteristic time – positional servomechanism undamped natural period ratios (r_v). Analog computer studies.

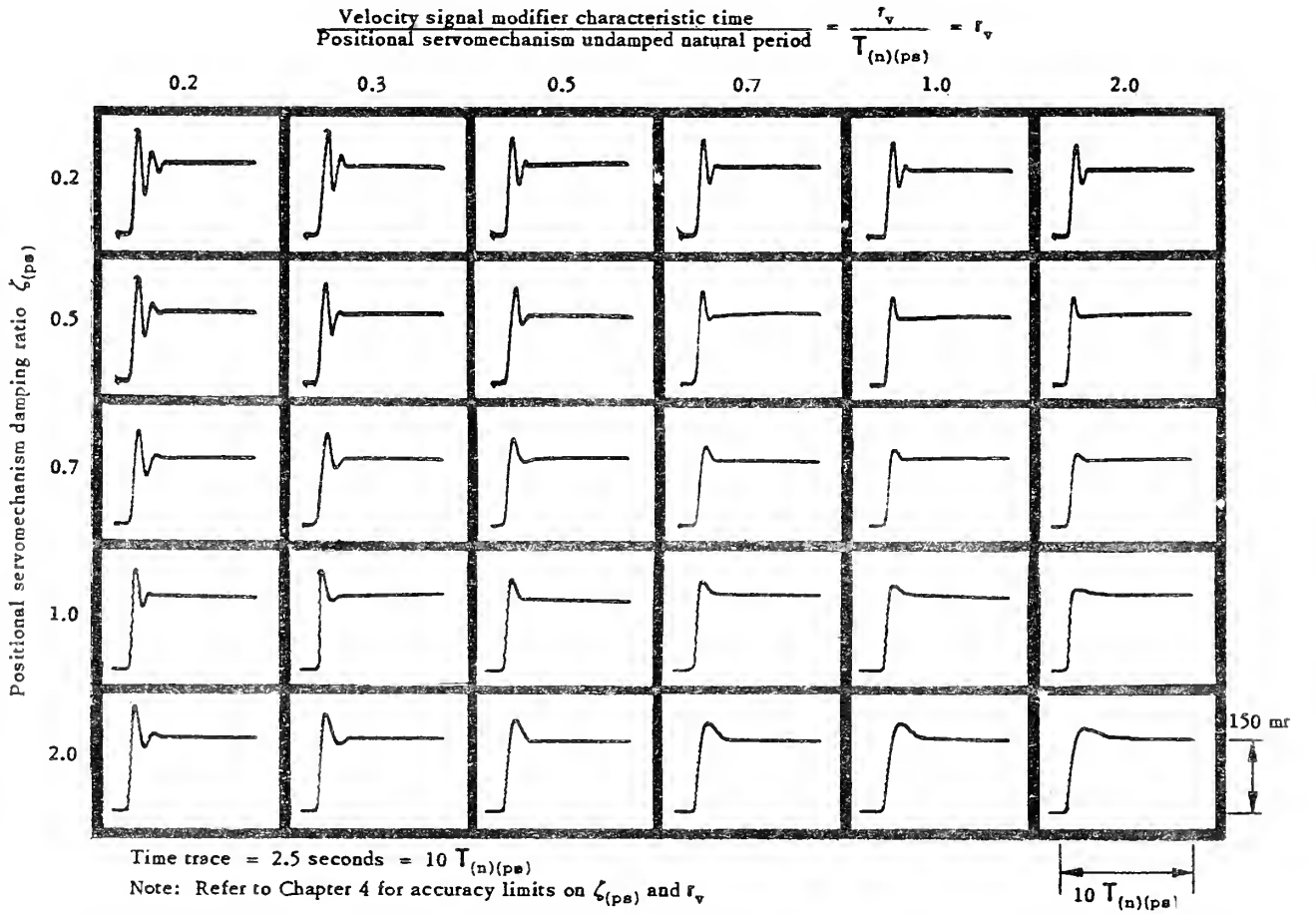

Fig. 23. Increasing step function response of modified velocity signal damping positional servomechanism (ps)(mvsd) for various damping ratios ($\zeta_{(ps)}$) and various velocity signal modifier characteristic time – positional servomechanism undamped natural period ratio (r_v). Cathode ray oscilloscope photographs of actual responses.

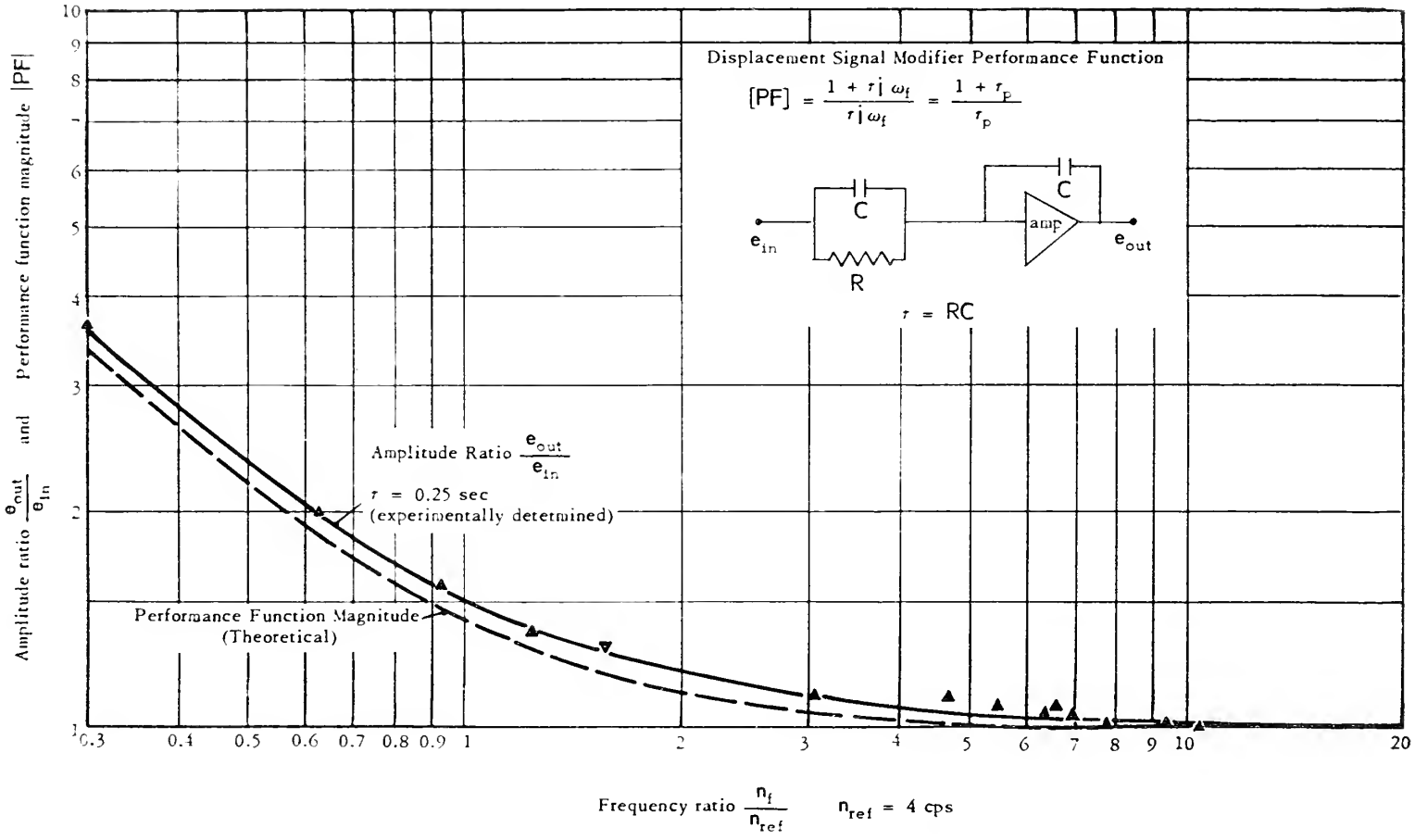

Fig. 24. Frequency response plot showing comparison of predicted and actual responses of the displacement signal modifier (dsm).

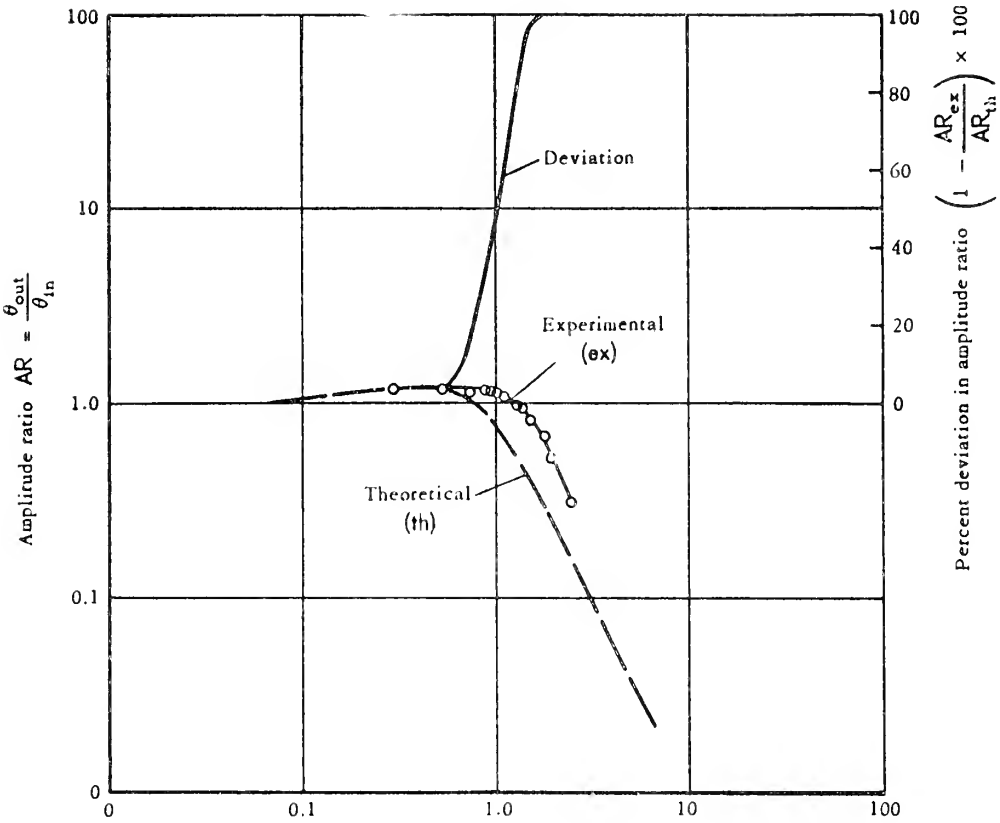

$$[PF]_{(ps)(mds)[AA]} = \frac{1 + 2\pi\tau_d\,'p}{2\pi\tau_d\,'p^3 + 2\zeta_{(ps)}2\pi\tau_d\,'p^2 + 2\pi\tau_d\,'p + 1}$$

$$'p = \frac{p}{\omega_{n(ps)}}$$

τ_d = 0.25 sec τ_d = 1.0 $\zeta_{(ps)}$ = 0.7

Fig. 25(a). Frequency response plot amplitude ratio vs frequency ratio for modified displacement signal, velocity signal damping positional servomechanism (ps)(vsd)(mds).

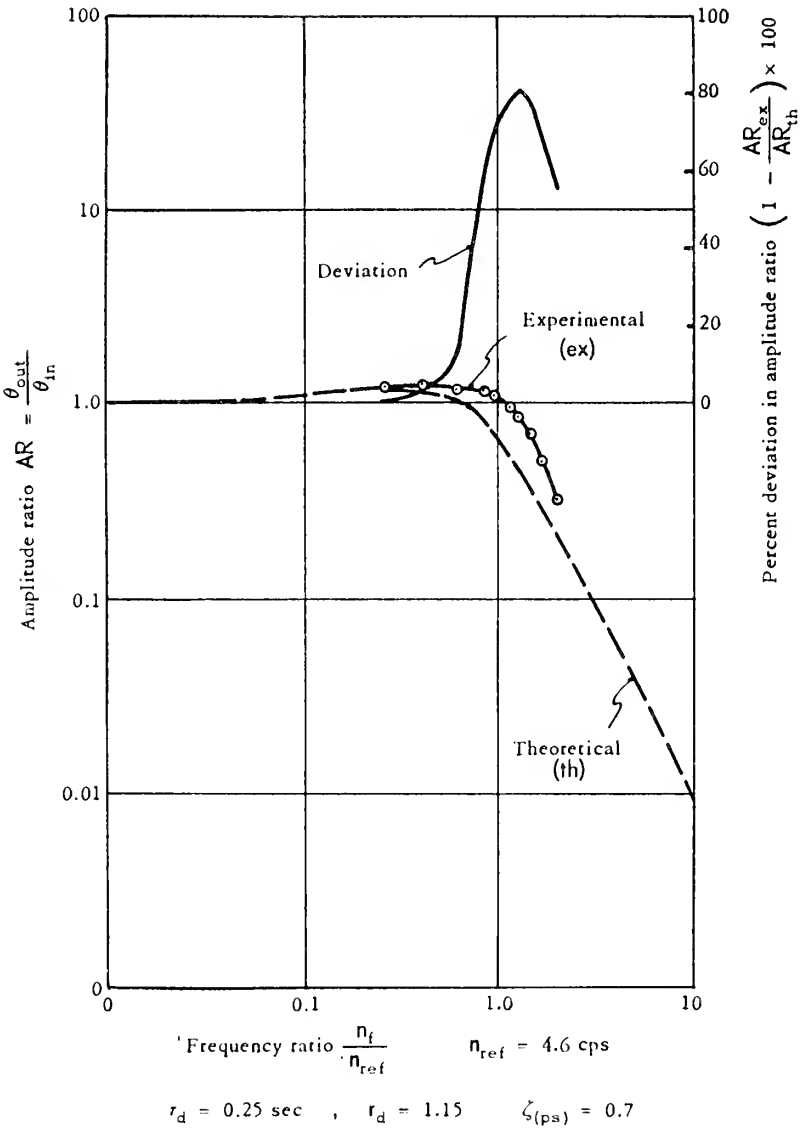

Fig. 25(b). Frequency response plot amplitude ratio vs frequency ratio for modified displacement signal, velocity signal damping positional servomechanism (ps) (vsd) (mds).

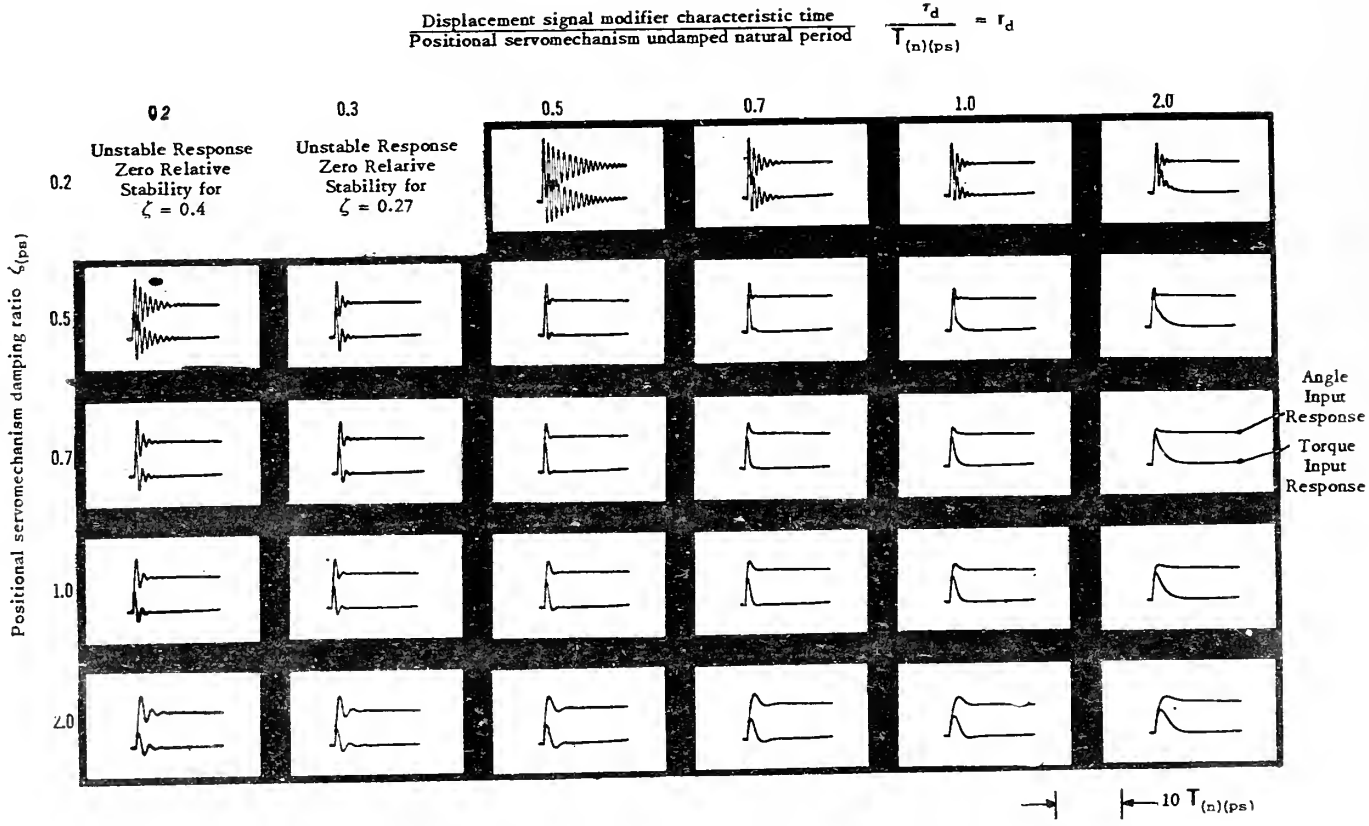

Reproduced from Massacbusetts Institute of Tecbnology Instrumentation Laboratory Report R-96 by Sidney Lees, December 1955 by courtesy of Professor Sidney Lees.

Fig. 26. Increasing step function responses and responses to a step input of interference torque for the modified displacement signal, velocity signal damping positional servomechanism (ps)(vsd)(mds), for various damping ratios ($\zeta_{(ps)}$) and various displacement signal modifier characteristic time – positional servomechanism undamped natural period ratios (r_d). Analog computer studies.

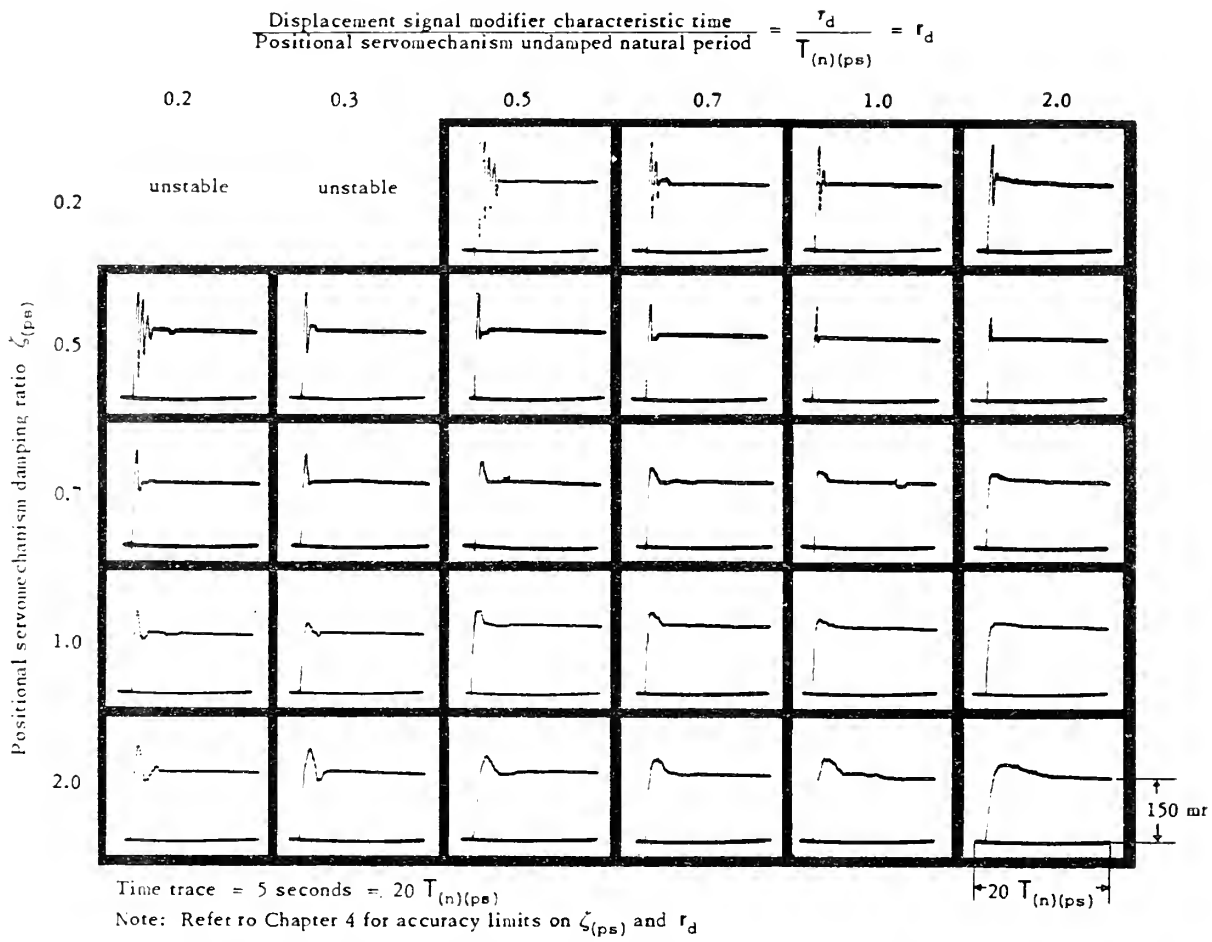

Fig. 27. Increasing step function response for the modified displacement signal, velocity signal damping positional servomechanism (ps) (vsd) (mds) for various damping ratios ($\zeta_{(ps)}$) and various displacement signal modifier characteristic time – positional servomechanism undamped natural period ratios (r_d). Cathode ray oscilloscope photographs of actual responses.

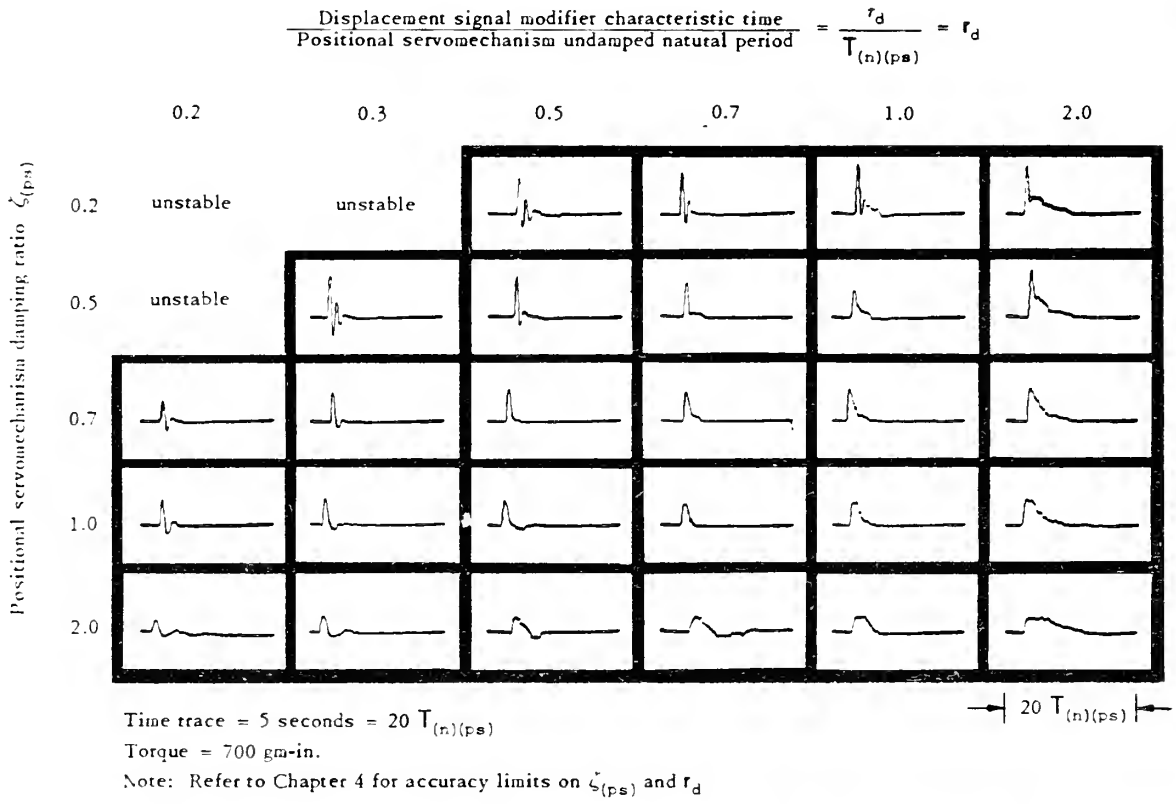

Fig. 28. Responses of modified displacement signal, velocity signal damping positional servomechanism (ps)(vsd)(mds) to a step input of torque applied at controlled member, for various damping ratios ($\zeta_{(ps)}$) and various displacement signal modifier characteristic time – positional servomechanism undamped natural period ratios (r_d). Cathode ray oscilloscope photographs of actual responses.

Positional servomechanism damping ratio $\zeta_{(ps)}$	Velocity signal modifier characteristic time-positional servomechanism undamped natural period ratio, r_v											
	0.2		0.3		0.5		0.7		1.0		2.0	
	Predicted	Actual	Predicted	Actual	Predicted	Actual	Predicted	Actual	Predicted	Actual	Predicted	Actual
0.2	75	40	67	54	65	47	60	35	55	51	55	40
	5-6	2.5	3-4	2.5	2-3	1.6	2-3	1.6	1.5-2.5	2.3	1.5-2.0	1.9
	6/6	2 2	5/5	2/2	3/3	1/1	3/3	1/1	3/3	2/1	3/3	1/1
0.5	65	52	62	48	54	40	40	40	35	25	25	25
	2-4	2.7	2-3	2.2	1-1.5	2.1	1-2	1.6	1-2	1.1	1-2	1.1
	4/3	2 2	2 2	2/1	1/1	1/1	1/1	1/0	1/0	1/0	1/0	1/0
0.7	58	46	42	40	37	31	29	21	25	13	15	10
	3-4	2.3	2-3	2.0	1.5-2.5	2.0	1-2	1.5	1-1.5	1.5	2-3	1.5
	3 3	2/1	2/1	1/1	1/1	1/1	1/0	1/0	1/0	1/0	1/0	1/0
1.0	56	45	46	40	35	27	30	15	25	12	12	8
	3-4	1.8	2-3	2.0	2-3	1.6	2	1.7	2	2.0	2-4	2.5
	3/2	2/1	2/1	1/1	1/1	1/0	1/0	1/0	1/0	1/0	1/0	1/0
2.0	53	45	46	35	42	30	33	20	29	20	15	14
	3-4	2.5-3	3-4	2-3	3-4	2.5	2-3	3.0	3	3.5	3-5	3-4.5
	3/3	2/1	2/2	1/1	1/1	1/0	1/0	1/0	1/0	1/0	1/0	1/0

percent overshoot
Response Time / $T_{(n)(ps)}$
Number overshoots / Number undershoots

$T_{(n)(ps)}$ based on using

$n_{(n)(ps)} = 4.0$ c.p.s.

Table I. Comparison between predicted and actual step function response for various values of $\zeta_{(ps)}$ and r_v for the modified velocity signal damping positional servomechanism (ps)(mvsd). Values taken from Sanborn recorder tape for actual response in place of Fig. 23 and from an enlargement of Fig. 22 for the predicted response.

Positional servomechanism damping ratio $\zeta_{(ps)}$	Displacement signal modifier characteristic time – positional servomechanism undamped natural period ratio r_d											
	0.2		0.3		0.5		0.7		1.0		2.0	
	Predicted	Actual	Predicted	Actual	Predicted	Actual	Predicted	Actual	Predicted	Actual	Predicted	Actual
0.2	UNSTABLE		UNSTABLE		90 — 18/18	60 3.5 5/4	85 3-5 9/9	60 3.2 3/3	65 3-4 6/5	55 2.0 2/2	55 2-4 5/4	55 4 2/1
0.5	80 8-10 10/9	60 2.8 3/3	70 2-4 4/3	56 2.5 2/1	55 1-2 2/2	54 2.0 1/1	50 1-2 2/1	47 1.5 1/1	30 1.5 1/1	45 1.0 1/1	20 1.0 1/1	35 .8 1/0
0.7	70 3-4 5/4	55 2-3 2/1	55 1.5-2 2/2	43 1-1.5 1/1	45 1 1/1	35 1.5 1/0	27 1 1/0	20 1.5 1/0	15-20 2 1/0	15 1.5-2.0 1/0	8 3-5 1/0	7 4-5 1/0
1.0	55 3-4 3/3	40 2.5 1/1	40 2-2.5 2/1	15 2.5 1/1	32 1.5-2 1/1	20 3-4 1/1	24 2 1/0	20 2.5 1/0	14 2-3 1/0	14 4 1/0	6 3-5 1/0	5 5-6 1/0
2.0	45 4-5 3/3	40 4-5 2/1	36 3-5 2/2	36 3-4 1/1	32 2.5-4 1/1	28 3-7 1/1	26 2-4 1/1	21 3-7 1/0	14 3-6 1/0	25 4-10 1/0	9 5-8 1/0	18 8-12 1/0

Percent overshoot
Response Time / $T_{(n)(ps)}$
number overshoots / number undershoots

$T_{(n)(ps)}$ based on using $n_{(n)(ps)}$ = 4.0 c.p.s.

Table II. Comparison between predicted and actual step function response for various values of $\zeta_{(ps)}$ and r_d for the Modified Displacement Signal, Velocity Signal Damping Positional Servomechanism (ps)(vsd)(mds). Values taken from enlargements of Figs. 26 and 27.

Positional servomechanism damping ratio $\zeta_{(ps)}$	Displacement signal modifier characteristic time – positional servomechanism undamped natural period ratio r_d											
	0.2		0.3		0.5		0.7		1.0		2.0	
	Predicted	Actual	Predicted	Actual	Predicted	Actual	Predicted	Actual	Predicted	Actual	Predicted	Actual
0.2	UNSTABLE		UNSTABLE		15-20 16/16	4-6 3/2	5-6 7/7	2.5 2/1	3-5 5/5	5-7 2/1	5-7 4/4	6-7 1/0
0.5	8 10/10	UN- STABLE	3-4 4/4	3-4 3/2	2-3 2/2	4-6 2/1	1.5-2 2/1	3 1/0	3-4 1/0	3 1/0	5-6 1/0	6-7 1/0
0.7	3-4 4/4	3-4 2/1	2 2/2	2-5 2/1	1.5-2 1/1	2-3 1/0	1.5-2 1/0	2-3 1/0	2-3 1/0	3-4 1/0	6-7 1/0	6-7 1/0
1.0	2-3 3/2	2-3 2/1	2-2.5 2/2	2.5-3 2/1	1.5-3 1/1	3-4 1/1	2 1/0	2 1/0	2-3 1/0	3.5 1/0	5-7 1/0	6-8 1/0
2.0	3-5 3/2	5-8 3/2	3-5 2/1	4-5 2/1	3-5 1/1	3-5 1/1	3.5-5 1/1	4-10 1/1	3-6 1/0	4 1/0	5-7 1/0	8-10 1/0

Response time
$T_{(n)(ps)}$
number overshoots
number undershoots

$T_{(n)(ps)}$ based on using $n_{(n)(ps)}$ = 4.0 c. p. s.

Table III. Comparison between predicted and actual response to a step input of torque for various values of $\zeta_{(ps)}$ and r_d for the modified displacement signal, velocity signal damping positional servomechanism (ps)(vsd)(mds). Values taken from enlargements of Figs. 26 and 28.

APPENDIX A

DERIVATION OF THE PERFORMANCE EQUATIONS FOR THE POSITIONAL SERVOMECHANISM CONFIGURATIONS TESTED

The basic equations for the positional servomechanism configurations shown in functional diagrams, Figs. 11, 12, and 13, are based on the assumptions that the components are perfect and that each component performance is characterized only by its sensitivity. The theoretical performance equations are derived by summing the torques acting on the torque summing member and setting the sum equal to zero. The torque generator, or motor, shaft is taken as the torque summing member. The development is based on general methods set forth in Volume I and II Instrument Engineering (6) and specific methods set forth by Lees (5).

A-1. Basic Positional Servomechanism Performance Equation

(ps)(b) [Velocity signal generator loop open - see Fig. 11.]

(a) Component performance equations:

(1) (sg) Signal generator:

$$e_{(dir)} = S_{(sg)}A_{(in)};\ e_{(fb)} = S_{(sg)}A_{(cm)} \qquad \text{(A-1)}$$

(2) (sc) Signal comparator:

$$e_{(sc)} = S_{(sc)}[e_{(dir)} - e_{(fb)}] = S_{(sc)}S_{(sg)}[A_{(in)} - A_{(cm)}]$$
$$= S_{(sc)}S_{(sg)}(C)A_{(cm)} \qquad \text{(A-2)}$$

(3) (vsc) Velocity signal comparator (includes adder circuit and chopper):

$$e_{(vsc)} = S_{(vsc)}e_{(sc)} = S_{(vsc)}S_{(sc)}S_{(sg)}(C)A_{(cm)} \qquad \text{(A-3)}$$

(4) (a) Amplifier:

$$e_a = S_a e_{(vsc)} = S_a S_{(vsc)}S_{(sc)}S_{(sg)}(C)A_{(cm)} \qquad \text{(A-4)}$$

(5) (tg) Torque generator:

$$M_{(tg)} = S_{(tg)[e:M]}{}^{e}a - S_{(tg)[\dot{A}:M]} \frac{d\,A_{(tsm)}}{dt}$$

$$M_{(tg)} = S_{(tg)[e:M]} S_a S_{(vsc)} S_{(sc)} S_{(sg)} (C) A_{(cm)} - S_{(tg)[\dot{A}:M]} \dot{A}_{(tsm)} \qquad \text{(A-5)}$$

where

$$\frac{dA}{dt} = \dot{A}; \quad \frac{d^2A}{dt^2} = \ddot{A}$$

(6) $(gt)_1$ Gear train to the controlled member:

$$A_{(tsm)} = S_{(gt)_1[A_{(gt)_1}:A_{(tsm)}]} A_{(gt)_1} = S_{(gt)_1} A_{(gt)_1} \qquad \text{(A-6)}$$

$$A_{(gt)_1} = A_{(cm)}$$

(7) $(gt)_2$ Gear train to the velocity signal generator:

$$A_{(tsm)} = S_{(gt)_2[A_{(gt)_2}:A_{(tsm)}]} A_{(gt)_2} = S_{(gt)_2} A_{(gt)_2} \qquad \text{(A-7)}$$

(b) Torque expressions:

(1) Inertia reaction torque:

$$M_{(ir)} = -\left(I_{(tsm)} + \frac{I_{(cm)}}{S^2_{(gt)_1}} + \frac{I_{(vsg)}}{S^2_{(gt)_2}} + I_{(gt)\,eff} \right) \ddot{A}_{(tsm)} \qquad \text{(A-8)}$$

$I_{(tsm)}$ = torque summing member inertia

$I_{(cm)}$ = control member inertia

$I_{(vsg)}$ = velocity signal generator inertia

$I_{(gt)\,eff}$ = effective gear trains inertia referred to the torque summing member.

(2) Viscous damping torque:

$$M_d = - c_{(d)(res)} \dot{A}_{(tsm)} \qquad \text{(A-9)}$$

$c_{(d)(res)}$ = residual viscous damping coefficient due to gears, bearings, and air damping.

(3) Torque generator torque:

$$M_{(tg)} = S_{(tg)[e:M]}S_a S_{(vsc)}S_{(sc)}S_{(sg)}{}^{(C)}A_{(cm)} - S_{(tg)[\dot{A}:M]}\dot{A}_{(tsm)} \tag{A-10}$$

(4) Interference torque at torque summing member:

$$M_{(intfr)(tsm)} = \frac{M_{(intfr)}}{S_{(gt)_1}} \tag{A-11}$$

(c) Torque summation about torque summing member:

$$M_{(ir)} + M_{(d)} + M_{(tg)} + M_{(intfr)(tsm)} = 0 \tag{A-12}$$

$$-\left[I_{(tsm)} + \frac{I_{(cm)}}{S^2_{(gt)_1}} + \frac{I_{(vsg)}}{S^2_{(gt)_2}} + I_{(gt)eff}\right]\ddot{A}_{(tsm)} - {}^{c}{}_{(d)(res)}\dot{A}_{(tsm)}$$

$$+S_{(tg)[e:M]}S_a S_{(vsc)}S_{(sc)}S_{(sg)}[A_{(in)} - A_{(cm)}] - S_{(tg)[\dot{A}:M]}\dot{A}_{(tsm)} + \frac{M_{(intfr)}}{S_{(gt)_1}} = 0 \tag{A-13}$$

but:

$$\begin{aligned} A_{(tsm)} &= S_{(gt)_1}A_{(gt)_1} = S_{(gt)_1}A_{(cm)} \\ \dot{A}_{(tsm)} &= S_{(gt)_1}\dot{A}_{(gt)_1} = S_{(gt)_1}\dot{A}_{(cm)} \\ \ddot{A}_{(tsm)} &= S_{(gt)_1}\ddot{A}_{(gt)_1} = S_{(gt)_1}\ddot{A}_{(cm)} \end{aligned} \tag{A-14}$$

Substituting Eq. (A-14) into (A-13), multiplying through by $S_{(gt)_1}$, and rearranging terms:

$$\left[I_{(cm)} + S^2_{(gt)_1}\left[I_{(tsm)} + \frac{I_{(vsg)}}{S^2_{(gt)_2}} + I_{(gt)(eff)}\right]\right]\ddot{A}_{(cm)} + S^2_{(gt)_1}\left[{}^{c}{}_{(d)(res)} + S_{(tg)[\dot{A}:M]}\right]\dot{A}_{(cm)}$$

$$+ \left[S_{(gt)_1}S_{(tg)[e:M]}S_{(a)}S_{(vsc)}S_{(sc)}S_{(sg)}\right]A_{(cm)}$$

$$= \left[S_{(gt)_1}S_{(tg)[e:M]}S_a S_{(vsc)}S_{(sc)}S_{(sg)}\right]A_{(in)} + M_{(intfr)} \tag{A-15}$$

Define:

$$I_{(cm)(eq)} = I_{(cm)} + S^2_{(gt)_1}\left[I_{(tsm)} + \frac{I_{(vsg)}}{S^2_{(gt)_2}} + I_{(gt)(eff)}\right]$$

= equivalent controlled member inertia (A-16)

$$S_{(ps)[\dot{A}:M]_{(res)}} = S^2_{(gt)_1}\left[c_{(d)(res)} + S_{(tg)[\dot{A}:M]}\right]$$

= positional servomechanism sensitivity for angular velocity input, torque output do to residual damping. (A-17)

$$S_{(ps)[A:M]} = \left[S_{(gt)_1} S_{(tg)[e:M]} S_{(a)} S_{(vsc)} S_{(sc)} S_{(sg)}\right]$$

= positional servomechanism sensitivity for angle input, torque output; equivalent to elastic coefficient and stiffness. (A-18)

$$\dot{A}_{(cm)} = \frac{d\,A_{(cm)}}{dt} = p\,A_{(cm)};\quad \ddot{A}_{(cm)} = \frac{d^2 A_{(cm)}}{dt^2} = p^2 A_{(cm)} \qquad (A\text{-}19)$$

Substituting Eqs. (A-16), (A-17), (A-18), (A-19) into Eq. (A-15) gives the performance equation:

$$\left[I_{(cm)(eq)}\,p^2 + S_{(ps)[\dot{A}:M]_{(res)}}\,p + S_{(ps)[A:M]}\right] A_{(cm)}$$

$$= S_{(ps)[A:M]}\,A_{(in)} + M_{(intfr)} \qquad (A\text{-}20)$$

Define:

$$\omega_{(n)(ps)} = \sqrt{\frac{S_{(ps)[A:M]}}{I_{(cm)(eq)}}}$$ = positional servomechanism undamped angular natural frequency (A-21)

$$n_{(n)(ps)} = \frac{\omega_{(n)(ps)}}{2\pi}$$ = positional servomechanism undamped natural frequency (A-22)

$$T_{(n)(ps)} = \frac{2\pi}{\omega_{(n)(ps)}}$$ = positional servomechanism undamped natural period (A-23)

$$\zeta_{(ps)(res)} = \frac{1}{2}\,\frac{S_{(ps)[\dot{A}:M](res)}}{\sqrt{S_{(ps)[A:M]} I_{(cm)(eq)}}}$$ = positional servomechanism residual damping ratio (A-24)

$$S_{(ps)[M:A]} = \frac{1}{S_{(ps)[A:M]}} = \text{positional servomechanism compliance.} \qquad \text{(A-25)}$$

With these parameters Eq. (A-20) now becomes:

$$\left[\frac{p^2}{\omega^2_{(n)(ps)}} + 2\zeta_{(ps)(res)}\frac{p}{\omega_{(n)(ps)}} + 1\right] A_{(cm)} = A_{(in)} + S_{(ps)[M:A]}M_{(intfr)} \qquad \text{(A-26)}$$

A-2. Velocity Signal Damping Positional Servomechanism

(ps)(vsd) performance equation [Velocity signal generator loop closed – see Fig. 11]

(a) Additional component performance equations

(1) (vsg) Velocity signal generator:

$$e_{(vsg)} = S_{(vsg)}\dot{A}_{(gt)_2} = \frac{S_{(vsg)}}{S_{(gt)_2}}\dot{A}_{(tsm)} \qquad \text{(A-27)}$$

(2) (vsa) Velocity signal amplifier:

$$e_{(vsa)} = S_{(vsa)}e_{(vsg)} = S_{(vsa)}\frac{S_{(vsg)}}{S_{(gt)_2}}\dot{A}_{(tsm)} \qquad \text{(A-28)}$$

(3) (vsc) Velocity signal comparator:

(Note: now with velocity signal generator loop closed)

$$e_{(vsc)} = S_{(vsc)}[e_{(sc)} - e_{(vsa)}]$$

$$e_{(vsc)} = S_{(vsc)}S_{(sc)}S_{(sg)}(C)A_{(cm)} - S_{(vsc)}S_{(vsa)}\frac{S_{(vsg)}}{S_{(gt)_2}}\dot{A}_{(tsm)} \qquad \text{(A-29)}$$

and then:

$$e_{(a)} = S_a e_{(vsc)} = S_a S_{(vsc)}S_{(sc)}S_{(sg)}(C)A_{(cm)} - S_a S_{(vsc)}S_{(vsa)}\frac{S_{(vsg)}}{S_{(gt)_2}}\dot{A}_{(tsm)} \qquad \text{(A-30)}$$

(b) Torque summation: $M_{(ir)} + M_{(d)} + M_{(tg)} + M_{(intfr)(tsm)} = 0$

(1) $M_{(tg)}$ is the only torque expression to change:

(2) $M_{(tg)} = S_{(tg)[e:M]}e_a - S_{(tg)[\dot{A}:M]}\dot{A}_{(tsm)}$

$$M_{(tg)} = S_{(tg)[e:M]} S_a S_{(vsc)} S_{(sc)} S_{(sg)} [A_{(in)} - A_{(cm)}]$$

$$- \left[S_{(tg)[e:M]} S_a S_{(vsc)} S_{(vsa)} \frac{S_{(vsg)}}{S_{(gt)_2}} + S_{(tg)[\dot{A}:M]} \right] \dot{A}_{(tsm)} \qquad \text{(A-31)}$$

Substituting Eq. (A-14) into Eq. (A-31), and multiplying through by $S_{(tg)_1}$:

$$S_{(gt)_1} M_{(tg)} = S_{(ps)[A:M]} (A_{(in)} - A_{(cm)})$$

$$- \left[S^2_{(gt)_1} S_{(tg)[e:M]} S_a S_{(vsc)} S_{(vsa)} \frac{S_{(vsg)}}{S_{(gt)_2}} + S^2_{(gt)_1} S_{(tg)[\dot{A}:M]} \right] \dot{A}_{(cm)}$$

(A-32)

Define:

$$S_{(ps)[\dot{A}:M]} = S^2_{(gt)_1} S_{(tg)[e:M]} S_a S_{(vsc)} S_{(vsa)} \frac{S_{(vsg)}}{S_{(gt)_2}} = \text{positional servomechanism sensitivity for angular velocity input, torque output} \qquad \text{(A-33)}$$

Therefore, by the same method as used to develop Eq. (A-20), the performance equation becomes:

$$\left[I_{(cm)(eq)} p^2 + (S_{(ps)[\dot{A}:M](res)} + S_{(ps)[\dot{A}:M]}) p + S_{(ps)[A:M]} \right] A_{(cm)}$$

$$= S_{(ps)[A:M]} A_{(in)} + M_{(intfr)} \qquad \text{(A-34)}$$

Define:

$$\zeta_{(ps)} = \frac{1}{2} \frac{S_{(ps)[\dot{A}:M]}}{\sqrt{S_{(ps)[A:M]} I_{(cm)(eq)}}} = \text{positional servomechanism damping ratio} \qquad \text{(A-35)}$$

Introducing the parameters of Eqs. (A-21), (A-24), (A-25) and (A-35) gives:

$$\left[\frac{p^2}{\omega^2_{(n)(ps)}} + [2 \zeta_{(ps)(res)} + 2\zeta_{(ps)}] \frac{p}{\omega_{(n)(ps)}} + 1 \right] A_{(cm)} = A_{(in)} + S_{(ps)[M:A]} M_{(intfr)} \qquad \text{(A-36)}$$

A-3. Modified Velocity Signal Damping Positional Servomechanism (ps)(mvsd), performance equation (see Fig. 12)

(a) Additional component performance equations:

(vsm) Velocity signal modifier:

$$e_{(vsm)} = S_{(vsm)} \frac{\tau_v p}{1 + \tau_v p} e_{(vsa)} \tag{A-37}$$

where

$$\tau_v = \text{velocity signal modifier characteristic time} \tag{A-38}$$

$$r_v = \frac{\tau_v}{T_{n(ps)}} = \text{velocity signal modifier characteristic time – positional servomechanism undamped natural period ratio.} \tag{A-39}$$

(b) Torque summation and performance equation:

Introducing the velocity signal modifier with the performance equation given by Eqs. (A-31) and (A-32) into the velocity signal feedback loop alters the expression of Eq. (A-32) as follows:

$$S_{(gt)_1} M_{(tg)} = S_{(ps)[A:M]}(A_{(in)} - A_{(cm)}) - \left(S_{(ps)[\dot{A}:M]} \frac{\tau_v p}{1 + \tau_v p} + S^2_{(gt)_1} S_{(tg)[\dot{A}:M]}\right) \dot{A}_{(cm)} \tag{A-40}$$

Therefore the performance equation becomes:

$$\left\{I_{(cm)(eq)} p^2 + \left(S_{(ps)[\dot{A}:M](res)} + S_{(ps)[\dot{A}:M]} \frac{\tau_v p}{1 + \tau_v p}\right) p + S_{(ps)[A:M]}\right\} A_{(cm)} = S_{(ps)[A:M]} A_{(in)} + M_{(intfr)} \tag{A-41}$$

Introducing the parameters of Eqs. (A-21), (A-24), (A-25) and (A-35)

$$\left\{\frac{p^2}{\omega^2_{n(ps)}} + \left(2\zeta_{(ps)(res)} + 2\zeta_{(ps)} \frac{\tau_v p}{1 + \tau_v p}\right) \frac{p}{\omega_{n(ps)}} + 1\right\} A_{(cm)} = A_{(in)} + S_{(ps)[M:A]} M_{(intfr)} \tag{A-42}$$

A-4. Modified Displacement Signal, Velocity Signal Damping Positional Servomechanism, (ps)(vsd)(mds), performance equations (see Fig. 13)

(a) Additional component performance equation:

(dsm) Displacement signal modifier:

$$e_{(dsm)} = S_{(dsm)} \quad \frac{1 + \tau_d p}{\tau_d p} \quad e_{(sc)} \tag{A-43}$$

Define:

$$\tau_d = \text{displacement signal modifier characteristic time} \tag{A-44}$$

$$r_d = \frac{\tau_d}{T_{n(ps)}} = \text{displacement signal modifier characteristic time – positional servomechanism undamped natural period ratio.} \tag{A-45}$$

(b) Torque summation and performance equation:

(1) The torque generator output in this model becomes:

$$M_{(tg)} = S_{(tg)[e:M]} S_a S_{(vsc)} S_{(sc)} S_{(sg)} \quad \frac{1 + \tau_d p}{\tau_d p} \; (C) \; A_{cm}$$

$$- \left[S_{(tg)[e:M]} S_a S_{(vsc)} S_{(vsa)} \quad \frac{S_{(vsg)}}{S_{(gt)_2}} + S_{(tg)[\dot{A}:M]} \right] \dot{A}_{(tsm)} \tag{A-46}$$

(2) Therefore the performance equations become:

$$\left\{ I_{(cm)(eq)} p^2 + (S_{(ps)[\dot{A}:M](res)} + S_{(ps)[\dot{A}:M]}) p + S_{(ps)[A:M]} \quad \frac{1 + \tau_d p}{\tau_d p} \right\} A_{(cm)}$$

$$= S_{(ps)[A:M]} \quad \frac{1 + \tau_d p}{\tau_d p} \quad A_{(in)} + M_{(intfr)} \tag{A-47}$$

$$\left\{ \frac{p^2}{\omega^2_{n(ps)}} + 2(\zeta_{(ps)(res)} + \zeta_{(ps)}) \quad \frac{p}{\omega_{n(ps)}} + \quad \frac{1 + \tau_d p}{\tau_d p} \right\} \quad A_{(cm)}$$

$$= \frac{1 + \tau_d p}{\tau_d p} \quad A_{(in)} + S_{(ps)[M:A]} M_{(intfr)} \tag{A-48}$$

Table A-1. Performance functions associated with the equation: $A_{(cm)} = [PF]_{(ps)[A;A]} A_{(in)} + [PF]_{(ps)[M;A]} M_{(intfr)}$.

Type Positional Servomechanism	$[PF]_{(ps)[A;A]}$	$[PF]_{(ps)[M;A]}$
Basic (b)	$\dfrac{1}{\dfrac{I_{(cm)(eq)}}{S_{(ps)[A;M]}} p^2 + \dfrac{S_{(ps)[\dot{A};M]res}}{S_{(ps)[A;M]}} p + 1} = \dfrac{1}{\left(\dfrac{p}{\omega_{n(ps)}}\right)^2 + 2\zeta_{(ps)(res)}\left(\dfrac{p}{\omega_{n(ps)}}\right) + 1}$	$S_{(ps)[M;A]}[PF]_{(ps)[A;A]}$
Velocity Signal Damping (vsd)	$\dfrac{1}{\dfrac{I_{(cm)(eq)}}{S_{(ps)[A;M]}} p^2 + \left(\dfrac{S_{(ps)[\dot{A};M]res} + S_{(ps)[\dot{A};M]}}{S_{(ps)[A;M]}}\right) p + 1} = \dfrac{1}{\left(\dfrac{p}{\omega_{n(ps)}}\right)^2 + 2\zeta_{(ps)(res)} + 2\zeta_{(ps)}\left(\dfrac{p}{\omega_{n(ps)}}\right) + 1}$	$S_{(ps)[M;A]}[PF]_{(ps)[A;A]}$
Modified Velocity Signal Damping (mvsd)	$\dfrac{1}{\dfrac{I_{(cm)(eq)}}{S_{(ps)[A;M]}} p^2 + \left(S_{(ps)[\dot{A};M](res)} + S_{(ps)[\dot{A};M]} \dfrac{\tau_v p}{1+\tau_v p}\right) p + 1} = \dfrac{1}{\left(\dfrac{p}{\omega_{n(ps)}}\right)^2 + \left(2\zeta_{(ps)(res)} + 2\zeta_{(ps)} \dfrac{\tau_v p}{1+\tau_v p}\right) \dfrac{p}{\omega_{n(ps)}} + 1}$	$S_{(ps)[M;A]}[PF]_{(ps)[A;A]}$
Velocity Signal Damping Modified Displacement Signal (vsd)(mds)	$\dfrac{\dfrac{1+\tau_d p}{\tau_d p} S_{(ps)[A;M]}}{I_{(cm)(eq)} p^2 + (S_{(ps)[\dot{A};M](res)} + S_{(ps)[\dot{A};M]}) p + \left(\dfrac{1+\tau_d p}{\tau_d p}\right) S_{(ps)[A;M]}} = \dfrac{\dfrac{1+\tau_d p}{\tau_d p}}{\left(\dfrac{p}{\omega_{n(ps)}}\right)^2 + (2\zeta_{(ps)(res)} + 2\zeta_{(ps)}) \left(\dfrac{p}{\omega_{n(ps)}}\right) + \dfrac{1+\tau_d p}{\tau_d p}}$	$\dfrac{\tau_d p}{1+\tau_d p} S_{(ps)[M;A]}[PF]_{(ps)[A;A]}$

Table A-2. Nondimensional performance functions associated with the equation: $A_{(cm)} = [PF]_{(ps)[A;A]} A_{(in)} + [PF]_{(ps)[M;A]} M_{(intfr)}$.

Type Positional Servomechanism	$[PF]_{(ps)[A;A]}$	$[PF]_{(ps)[M;A]}$
Basic (b)	$\frac{1}{'p^2 + 2\zeta_{(ps)(res)}\,'p + 1}$	$S_{(ps)[M;A]}[PF]_{(ps)[A;A]}$
Velocity Signal Damping (vsd)	$\frac{1}{'p^2 + (2\zeta_{(ps)(res)} + 2\zeta_{(ps)})\,'p + 1}$	$S_{(ps)[M;A]}[PF]_{(ps)[A;A]}$
Modified Velocity Signal Damping (mvsd)	$\frac{1}{'p^2 + \left(2\zeta_{(ps)(res)} + 2\zeta_{(ps)}\frac{2\pi r_v\,'p}{1+2\pi r_v\,'p}\right)'p + 1} = \frac{1+2\pi r_v\,'p}{2\pi r_v\,'p^3 + [2\pi r_v(\zeta_{(ps)(res)} + \zeta_{(ps)}) + 1]\,'p^2 + (2\zeta_{(ps)(res)} + 2\pi r_v)\,'p + 1}$	$S_{(ps)[M;A]}[PF]_{(ps)[A;A]}$
Velocity Signal Damping Modified Displacement Signal (vsd)(mds)	$\frac{\frac{1+2\pi r_d\,'p}{2\pi r_d\,'p}}{'p^2 + (2\zeta_{(ps)(res)} + 2\zeta_{(ps)})\,'p + \frac{1+2\pi r_d\,'p}{2\pi r_d\,'p}} = \frac{1+2\pi r_d\,'p}{2\pi r_d\,'p^3 + 2\pi r_d(2\zeta_{(ps)(res)} + 2\zeta_{(ps)})\,'p^2 + 2\pi r_d\,'p + 1}$	$\frac{2\pi r_d\,'p}{1+2\pi r_d\,'p} S_{(ps)[M;A]}[PF]_{(ps)[A;A]}$

Note: $'p = \frac{p}{\omega_{n(ps)}}$ = nondimensional derivative operator

$r_v = \frac{\tau_v}{T_{n(ps)}}$ = velocity signal modifier characteristic time – positional servomechanism undamped natural period ratio

$r_d = \frac{\tau_d}{T_{n(ps)}}$ = displacement signal modifier characteristic time – positional servomechanism undamped natural period ratio

APPENDIX B

CALCULATIONS FOR SENSITIVITIES AND SYSTEM PARAMETERS

Actual systems built with physical components can not be expected to perform as well as a theoretical model. Components of the theoretical model are considered to be perfect and to perform according to mathematical concept assigned to each, for all ranges of and variation in the input.

In order to predict the performance of the system, the mathematical concept of each component or group of components must be known, determined, or set within reasonable tolerances. This can be done within certain limitations due to uncertainties inherent in physical components and in taking measurements.

B-1. The equivalent moment of inertia at the controlled member, $I_{(cm)(eq)}$, and the residual damping coefficient measured at the controlled member. $C_{(d)(res)cm} = S_{(gt)1}\ C_{d(res)}$, are calculated as follows based on data plotted in Figs. 14a and 14b and obtained from the moment of inertia determination test described in Chapter 4.

$$I_{(cm)(eq)}\ddot{A}_{(cm)} + C_{d(res)(cm)}\dot{A}_{(cm)} + k_{(sp)}\ A_{cm} = k_{(sp)}A_{in} \qquad \text{(B-1)}$$

$k_{(sp)}$ = stiffness of the auxiliary springs
= 542.5 inch-oz/rad (see Fig 14a) (B-2)

$$\omega_{n(aux)} = \sqrt{\frac{k_{(sp)}}{I_{(cm)eq}}} = \text{undamped angular natural frequency of the system with auxiliary springs attached}$$

= 39.3 rad/sec (see Fig. 14b) (B-3)

therefore:

$$I_{(cm)(eq)} = \frac{k_{(sp)}}{\omega^2_{n(aux)}} = 135 \text{ oz-in}^2 \qquad \text{(B-4)}$$

$$= .35 \text{ oz-in sec}^2$$

$$\zeta_{(aux)} = \frac{C_{(d)(res)(cm)}}{k_{(sp)}} \times \frac{\omega_{n(aux)}}{2} = \text{damping ratio of the system with auxiliary springs attached} \qquad \text{(B-5)}$$

From Fig. 14b the transient peak ratio between successive peaks averages 0.93. Using transient peak ratio curves of page 257, Volume II (6) gives:

$$\zeta_{(aux)} = 0.025 \tag{B-6}$$

This value is subject to inaccuracies in measurement and to the assumption that a true second order system exists. Therefore:

$$C_{(d)(res)(cm)} = S^2_{(gt)1} C_{d(res)} = \frac{2\,\zeta_{(aux)} k_{(sp)}}{\omega_{n(aux)}} = 0.7\ \frac{\text{in-oz}}{\text{rad/sec}} \tag{B-7}$$

B-2. The component sensitivities are subject to variation because of inherent uncertainties existing in physical units. Each component sensitivity is determined either by direct measurement and calculation of test data on that component alone, or by test data obtained on a group of components in conjunction with tests made on individual components of that group. If a component sensitivity is subject to large variations, a nominal sensitivity representative of the operating range is assumed.

(a) The gear train sensitivities are determined by counting the gear teeth on each gear and multiplying the mesh ratios together.

$$S_{(gt)[A_{(gt)1};A_{(tsm)}]} = S_{(gt)1} = \frac{100}{32} \times \frac{100}{18} = 17.35$$

$$S_{(gt)[A_{(gt)2};A_{(tsm)}]} = S_{(gt)2} = \frac{100}{32} \times \frac{74}{18} = 12.82 \tag{B-8}$$

(b) The torque generator sensitivity $S_{(tg)[e;M]}$ is calculated from data based on the static stiffness test and error signal to amplifier output test shown in Fig. 15. These tests are described in Chapter 4.

$$S_{(ps)[A;M]} = [S_{(sg)}S_{(sc)}S_{(vsc)}S_{(a)}]\, S_{(gt)1}S_{(tg)[e;M]} \text{ (see A-18)} \tag{B-9}$$

$$S_{(ps)[A;M]} = 243\ \frac{\text{oz-in}}{\text{rad}} \text{ (Calculated from Fig. 15)} \tag{B-10}$$

$$S_{(sg)}S_{(sc)}S_{(vsc)}S_{(a)} = 240\ \frac{\text{volts}}{\text{radian}} \quad \text{(Calculated from Fig. 15)} \tag{B-11}$$

therefore:

$$S_{(tg)[e;M]} = \frac{S_{(ps)[A;M]}}{[S_{(sg)}S_{(sc)}S_{(vsc)}S_a]} = .058\ \frac{\text{oz-in}}{\text{volt}} \tag{B-12}$$

Calculated values of $S_{(tg)[e;M]}$ from Fig. 9 are as follows:

$$S_{(tg)[e;M]} = .05 \frac{oz\text{-}in}{volt} \text{ (at zero R.P.M. from 0 to 15 volts)}$$

$$S_{(tg)[e;M]} = .075 \frac{oz\text{-}in}{volt} \text{ (at zero R.P.M. from 100 to 115 volts)}$$

$$S_{(tg)[e;M]} = .032 \frac{oz\text{-}in}{volt} \text{ (at 800 R.P.M. from 0 to 15 volts)}$$

$$S_{(tg)[e;M]} = .064 \frac{oz\text{-}in}{volt} \text{ (at 800 R.P.M. from 100 to 115 volts)}$$

Therefore the calculated value (B-12), falls within the values determined from the motor characteristic curves of Fig. 9. The latter values are cited because they represent the low and high operating range of the motor in the system.

(c) The signal generator sensitivity, $S_{(sg)}$, is calculated as follows:

Potentiometer excitation voltage = 78 volts

Range of operation of linear potentiometers = 10 turns

therefore:

$$S_{(sg)} = \frac{78}{(10 \times 2\pi)} = 1.24 \frac{volts}{radian} \qquad \text{(B-13)}$$

(d) The signal comparator sensitivity, $S_{(sc)}$, is taken as unity since the signal comparator is an integral part of the input and output signal generator circuit scheme rather than an individual component.

(e) The sensitivity of the A.C. amplifier and velocity signal comparator combination is calculated from (B-11) to be as follows:

$$S_{(vsc)}S_{(a)} = \frac{240}{1.24} = 193.5 \frac{volts}{volt} \qquad \text{(B-14)}$$

The sensitivity of the amplifier was measured at $S_{(a)}$ = 3000 to 4000 volts/volt. From Fig. 8b $S_{(vsc)}$ is calculated to be from 0.1 to 0.040 volts/volt over the expected operating range of input voltages resulting in:

$$S_{(vse)}S_a = 160 \frac{volts}{volt}$$

to

$$S_{(vsc)}S_a = 392 \frac{volts}{volt} \qquad \text{(B-15)}$$

Therefore the calculated value of $S_{(vsc)}S_{(a)}$ in (B-14) compares favorably with the range of values calculated in (B-15).

(f) The sensitivity of the velocity signal generator is calculated from the slope of the tachometer output voltage vs speed curves of Fig. 10 to be:

$$S_{(vsg)} = \frac{39}{\frac{(1800)}{60} \times 2\pi} = .207 \frac{\text{volts}}{\text{rad/sec}} \qquad \text{(B-16)}$$

(g) The velocity signal attenuator is a voltage divider consisting of a 5000 ohm (5K) variable resistor. The sensitivities of the velocity signal attenuator for the damping ratios set are calibrated as follows:

Servo Set For ζ_{PS}	$R_{Attenuator}$ (measured ohms)	$S_{(vsa)} = \frac{R_{Att.}}{5K}$ Volts/volt
Basic System	0	0
0.2	0.31K	0.062
0.5	0.60K	0.120
0.7	1.16K	0.232
1.0	1.85K	0.370
2.0	3.75K	0.750

(h) The torque generator sensitivity $S_{(tg)[\dot{A};M]}$ which accounts for back e.m.f. effects varies with speed and control field voltage. This sensitivity varies as follows:

$$S_{(tg)[\dot{A};M]} = \frac{.40}{\frac{1800}{60} \times 2\pi} = .002 \frac{\text{oz-in}}{\text{rad/sec}} \quad \text{(at low speed control voltage 10 to 15 volts)}$$

$$S_{(tg)[\dot{A};M]} = \frac{.25}{\frac{600}{60} \times 2\pi} = .004 \frac{\text{oz-in}}{\text{rad/sec}} \quad \text{(at 800 RPM control voltage 10 to 15 volts)}$$

$$S_{(tg)[\dot{A};M]} = \frac{.40}{\frac{600}{60} \times 2\pi} = .006 \frac{\text{oz-in}}{\text{rad/sec}} \quad \text{(at low RPM control voltage 50 to 75 volts)}$$

$$S_{(tg)[\dot{A};M]} = \frac{.48}{\frac{500}{60} \times 2\pi} = .009 \frac{\text{oz-in}}{\text{rad/sec}} \quad \text{(at 800 RPM control voltage 50 to 75 volts)}$$

$$S_{(tg)[\dot{A};M]} = .002 \frac{\text{oz-in}}{\text{rad/sec}} \tag{B-17}$$

is taken as the nominal value of sensitivity because normal operation is expected to be in the low speed, low voltage region of the motor during test.

B-3 The predicted undamped natural frequency $n_{(ps)}$ and damping ratio $\zeta_{(ps)}$ for the basic positional servomechanism and for the basic positional servomechanism with velocity signal damping shown in Fig. 11 are calculated as follows from equations derived in Appendix A and values determined in this appendix.

$$n_{n(ps)} = \frac{\omega_{n(ps)}}{2\pi} = \frac{1}{2\pi} \sqrt{\frac{S_{(ps)[A;M]}}{I_{(cm)(eq)}}} \tag{B-18}$$

$$S_{(ps)]A;M]} = 243 \frac{\text{oz-in}}{\text{rad}} \qquad I_{(cm)eq} = .35 \text{ oz in sec}^2$$

$$n_{n(ps)} = 4.2 \text{ cycles/second} \tag{B-19}$$

$$S_{(ps)[\dot{A};M]_{(res)}} = S^2_{(gt)1} C_{(d)(res)} + S_{(tg)[\dot{A};M]} = 1.3 \frac{\text{oz-in}}{\text{rad/sec}} \tag{B-20}$$

$$S_{(ps)[\dot{A};M]} = S^2_{(gt)1} S_{(tg)[e;M]} S_a S_{(vsc)} S_{(vsa)} \frac{S_{(vsg)}}{S_{(gt)2}} = 55.2 S_{(vsa)} \tag{B-21}$$

$$\zeta = (\zeta_{(ps)res} + \zeta_{(ps)}) = \frac{1}{2} \frac{S_{(ps)[\dot{A};M]_{(res)}} + S_{(ps)[\dot{A};M]}}{\sqrt{S_{(ps)[A;M]} I_{(cm)eq}}}$$

Therefore the predicted or calculated and the observed damping ratios are shown below:

ζ desired	$S_{(vsa)}$	$S_{(ps)[\dot{A};M]}$	$1.3 + S_{[\dot{A};M]}$	ζ Calc.	ζ Obs.	difference
(Basic system)	0	0	1.3	.072	.07 – .09	3 – 25%
.2	.062	3.42	4.72	.255	.23	+ 10%
.5	.112	6.18	7.48	.404	.45	– 11%
.7	.232	12.80	14.1	.76	.7	+ 8%
1.0	.370	20.40	21.7	1.17	1.1	+ 6%
2.0	.750	41.4	42.7	2.31	2.1	+ 9%

$$\text{difference} = \frac{\text{calc.} - \text{obs.}}{\text{calc.}}$$

Note: The observed values for damping ratio were obtained from increasing step responses. Lither response time RT or transient peak ratio TPR measurements or both were used to calculate the observed value. Since measurement of damping ratio is open to uncertainty and since for a given calibration of the servo, two successive runs may differ slightly, the calibration required to obtain any one damping ratio was based on a $S_{(vsa)}$ setting that gave an average damping ratio (for many responses) equal to that ratio desired. Tolerances on damping ratio measurement are described in Chapter 4.

BIBLIOGRAPHY

1. "Automatic Feedback Control," by William R. Ahrendt and John F. Taplin, McGraw-Hill Book Company, Inc., New York, N. Y., First Edition, 1951.
2. "Elements of Servomechanism Theory," by George J. Thaler, McGraw-Hill Book Company, Inc., New York, N. Y., 1955.
3. "Servomechanisms and Regulating System Design," by Harold Chestnut and Robert W. Mayer, John Wiley and Sons, Inc., New York, N. Y., 1955.
4. "Servomechanism Practice," by William R. Ahrendt, McGraw-Hill Book Company, Inc., New York., N. Y., 1954.
5. "Design Basis for Multiloop Positional Servomechanisms," by Sidney Lees, A. S. M. E. Paper No. 55-A-126, 1955.
6. "Instrument Engineering," by Charles S. Draper, Walter McKay, and Sidney Lees, McGraw-Hill Book Company, Inc., New York, N. Y., First Edition, Vol. I, 1952, Vol. II, 1953 and Vol. III, 1955.
7. "Evaluating the Effect of Nonlinearity in a Two-Phase Servomotor," by W. A. Stein and G. J. Thaler, A. I. E. E. Transaction Paper No. 54-522, January 1955.